



MARINET

Marine Renewables Infrastructure Network

D2.4: Collation of off-shore wind-wave dynamics

Author(s):

| | |
|----------------|----------|
| H. Bredmose | DTU WIND |
| S. E. Larsen | DTU WIND |
| D. Matha | USTUTT |
| A. Rettenmeier | USTUTT |
| E. Marino | UNIFI |
| L. Sættran | NTNU |

Revision: 02
Date: 30 November 2012













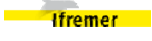

















ABOUT MARINET

MARINET (Marine Renewables Infrastructure Network for Emerging Energy Technologies) is an EC-funded consortium of 29 partners bringing together a network of 42 specialist marine renewable energy testing facilities. MARINET offers periods of free access to these facilities at no cost to research groups and companies. The network also conducts coordinated research to improve testing capabilities, implements common testing standards and provides training and networking opportunities in order to enhance expertise in the industry. The aim of the MARINET initiative is to accelerate the development of marine renewable energy technology.

Companies and research groups who are interested in availing of access to test facilities free of charge can avail of a range of infrastructures to test devices at any scale in areas such as wave energy, tidal energy and offshore-wind energy or to conduct specific tests on cross-cutting areas such as power take-off systems, grid integration, moorings and environmental data. In total, over 700 weeks of access is available to an estimated 300 projects and 800 external users.

MARINET is consists of five main areas of focus or 'Work Packages': Management & Administration, Standardisation & Best Practice, Transnational Access & Networking, Research and Training & Dissemination. The initiative runs for four years until 2015.

Partners

| | | | |
|---|---|---|--|
|    | <p>Ireland University College Cork, HMRC (UCC_HMRC) <i>Coordinator</i> Sustainable Energy Authority of Ireland (SEAI_OEDU)</p> | <p>Netherlands Stichting Tidal Testing Centre (TTC) Stichting Energieonderzoek Centrum Nederland (ECNeth)</p> |   |
|  | <p>Denmark Aalborg Universitet (AAU) Danmarks Tekniske Universitet (RISOE)</p> | <p>Germany Fraunhofer-Gesellschaft Zur Foerderung Der Angewandten Forschung E.V (Fh_IWES) Gottfried Wilhelm Leibniz Universität Hannover (LUH) Universitaet Stuttgart (USTUTT)</p> |    |
|   | <p>France Ecole Centrale de Nantes (ECN) Institut Français de Recherche Pour l'Exploitation de la Mer (IFREMER)</p> | <p>Portugal Wave Energy Centre – Centro de Energia das Ondas (WavEC)</p> |  |
|        | <p>United Kingdom National Renewable Energy Centre Ltd. (NAREC) The University of Exeter (UNEXE) European Marine Energy Centre Ltd. (EMEC) University of Strathclyde (UNI_STRATH) The University of Edinburgh (UEDIN) Queen's University Belfast (QUB) Plymouth University (PU)</p> | <p>Italy Università degli Studi di Firenze (UNIFI-CRIACIV) Università degli Studi di Firenze (UNIFI-PIN) Università degli Studi della Tuscia (UNI_TUS) Consiglio Nazionale delle Ricerche (CNR-INSEAN)</p> |     |
|   | <p>Spain Ente Vasco de la Energía (EVE) Tecnalia Research & Innovation Foundation (TECNALIA)</p> | <p>Norway Sintef Energi AS (SINTEF) Norges Teknisk-Naturvitenskapelige Universitet (NTNU)</p> |   |
|  | <p>Belgium 1-Tech (1_TECH)</p> | | |



Acknowledgements

The research leading to these results has received funding from the European Union Seventh Framework Programme (FP7) under grant agreement no. 262552.

Legal Disclaimer

The views expressed, and responsibility for the content of this publication, lie solely with the authors. The European Commission is not liable for any use that may be made of the information contained herein.



REVISION HISTORY

| Rev. | Date | Description | Author | Checked by |
|-------------|-------------|--------------------|------------------------------|-------------------|
| 01 | 31/10 2012 | Draft | H. Bredmose and S. E. Larsen | Self-checked |
| 02 | 30/11 2012 | Final | H. Bredmose and S. E. Larsen | Cross-checked |
| | | | | |
| | | | | |
| | | | | |
| | | | | |
| | | | | |

EXECUTIVE SUMMARY

The present report constitutes the Protocol Manual for ensuring harmonisation of offshore wind and wave simulation being implemented at MaRINET facilities. Wind and wave climates for five offshore wind sites in the North Sea and the Baltic Sea have been presented in terms of probability distributions for wind speed along with a series of lumped sea states and turbulence intensity values, parameterised with respect to the wind speed. Further, extreme values for wind speed and significant wave height have been provided.

Further to the wind distributions and lumped characteristics, the Weibull parameters for the wind distribution and explicit formulas for the turbulence intensity and significant wave height are provided. For the correlation of wave peak period and significant wave height, a standard formula from the IEC-61400-3 code have been found to cover the scatter in the data, although one coefficient in this formula must be decided upon by the user. Further, the value of γ , the JONSWAP peak enhancement parameter must be chosen by the user. This can be done either from an explicit formula or by the standard choices of $\gamma=1.0$ or $\gamma=3.3$. Hereby a full description of a unidirectional wind-wave climate can be constructed. If needed, this climate can be supplemented by the user with the combined directional distribution of wind and waves, either based on data or in terms of parametric studies.

The scaling method proposed is the dynamic-elastic scaling, which maintains the ratios between hydrodynamic, aerodynamic, stiffness-induced and gravitational forces. This scaling preserves the Froude number for the water phase and the tip speed ratio for the rotor. The Reynolds numbers for air and water, however, are not conserved. A redesign of the model-scale blades will therefore be needed. Here the scaled thrust-curve must be matched. Further, if possible, the torque from the airfoil should be matched. This requirement, however, is difficult to achieve due to the change in lift/drag ratio at low Reynolds number. It is therefore foreseen, that the aerodynamic torque and thus produced power will not be scaled correctly. As a consequence, roll-forcing induced by the dynamic change in generator moment will not scale correctly. However, the correct scaling of rotor thrust is found to have higher priority and thus justifies the scaling choice.

An example of down-scaling of wind and wave conditions has been supplied. The example also demonstrates how the structure (a floating wind turbine) should be scaled. It is demonstrated that the proposed scaling yields model-scale results for thrust- and wave- induced motion that can be up-scaled to prototype scale with a perfect match.

CONTENTS

| | | |
|----------|--|-----------|
| 1 | INTRODUCTION | 7 |
| 2 | CHARACTERISTICS OF OFFSHORE WIND –WAVE CLIMATE. | 8 |
| 2.1 | SOURCES OF DATA..... | 8 |
| 2.2 | PARAMETERS FOR WIND AND WAVE SPECIFICATION | 9 |
| 2.3 | ONE –PARAMETER CLIMATE BASED ON WIND SPEED. | 10 |
| 2.4 | STANDARD OFFSHORE CONDITIONS FOR TESTING AND MODELLING | 21 |
| 3 | SCALING OF WIND AND WAVE CONDITIONS FOR PHYSICAL MODEL TEST..... | 29 |
| 3.1 | REVIEW OF EXISTING SCALING STUDIES AND RELEVANT NONDIMENSIONAL NUMBERS | 29 |
| 3.2 | RECOMMENDED SCALING METHOD | 33 |
| 3.3 | SCALING OF WIND AND WAVE CLIMATE PARAMETERS | 38 |
| 3.4 | EXAMPLE: SCALED EXPERIMENT OF A FLOATING WIND TURBINE | 38 |
| 3.5 | DISCUSSION | 46 |
| 4 | CONCLUSIONS AND RECOMMENDATIONS | 47 |
| 5 | REFERENCES..... | 48 |

1 INTRODUCTION

The aim of this report is to constitute a protocol manual to ensure harmonisation of offshore wind and wave simulation at facilities within the MaRINET project.

Basically, the presentation is organised into two parts:

In section 2, we review the information that is available in international standards, reports and papers describing data sets, information and procedures regarding environmental parameters that must be specified for offshore wind turbines. The review is specifically focused on parameters that are often handled also within laboratory facilities meaning that focus is on the wind and wave parameters. In section 2.4 the review is condensed into a recommendation for a set of standard wind and wave climates, which are suitable for generic use. It is emphasised that these climates are not intended to form a design basis for any real structure.

In section 3, we review the scaling necessary for physical model tests with simultaneous wind and waves. The necessary considerations for dynamic-elastic scaling is introduced and applied to the wind and wave fields for a floating wind turbine. An example of down-scaling a wind-wave climate to model scale and up-scaling of the model-results to prototype scale is given. The results and implications are discussed.

Finally section 4 and 5 contain the overall conclusion and the references respectively.

2 CHARACTERISTICS OF OFFSHORE WIND – WAVE CLIMATE.

In the present section, we consider the current specification of the offshore wind and wave climate for design purposes. We mention other parameters that would be part of an offshore observation system, but would only rarely enter into tests in laboratory facilities due to modelling difficulties. Finally, the climate specifications from five specific sites are compared and a generic description is devised.

2.1 SOURCES OF DATA

The main data sources for this report are the design basis from the EU-UpWind project [1]. The report gives met-ocean data from two sites in the North Sea. One site, Ijmuiden Munitiestort, is a shallow water site with 21 meter water depth. The other site, K13 of 25 m depth is also denoted a shallow water site. After suitable supplement of data from an additional wave buoy at 50 m depth, the K13 data are further argued to reflect a nominal depth of 50 m, since the larger depth will mainly be important for the extreme wave heights [1]. In the following we shall shorten Ijmuiden Munitiestort to simply Ijmuiden.

The UpWind site locations are shown in Figure 2.1.1.

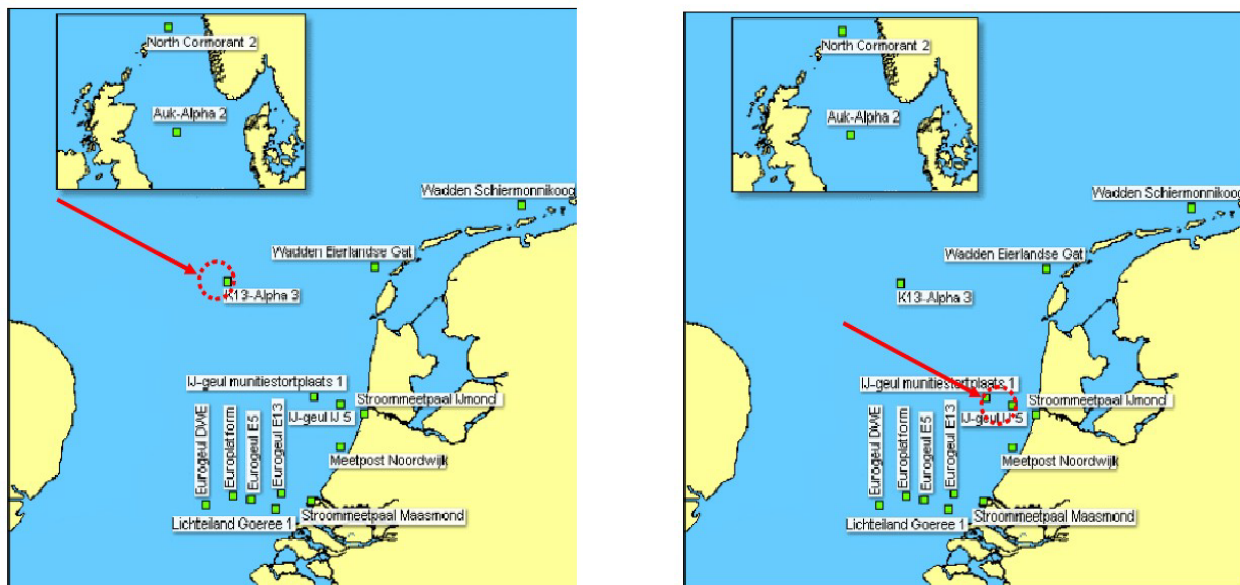


Figure 2.1.1. UpWind sites for the data sampling for design basis studies. Left: K13, serving both as deep water and shallow water site. Right: Ijmuiden Munitiestort shallow water site. From [1].

Additional to the data from the UpWind the present report draws from a number of standards developed for the offshore wind energy industry, notably IEC-61400-3 [2], DNV:OJ-J101 [3] and ABS [4]. Further, additional data are added from other EU-projects, notably the EU-DOWNVIND (with the Beatrice and the Södra Midsjöbanken) and the EU-NORSEWIND projects. The positions of the four associated locations are shown in Figure 2.1.2.



Figure 2.1.2. Full overview of locations referred to in this report, The sites are: Ijmuiden:1, K13:2, Beatrice:3 and Södra Midsjöbanke: 4. For the two first see the more detailed figure 2.1.1.

The wind and wave data presented in this study thus provide examples from sites in the North Sea and Baltic Sea and further illustrate the variability between the locations. For some parameters and relations, notable similarities are observed and might thus represent general climate characteristics with wider applicability. Here, however, it must be emphasized that the applicability of such general relations are only valid to the extent that no explicit and implicit assumptions of the applied models are violated. Examples of such violating aspects could be depth limitations, wave refraction, fetch conditions for wind generation of waves and inadequate wind shear description.

With the above in mind, for full design basis activities, the importance of site specific data cannot be over-stated. In this context, an obvious miss in the data sets from a European climate point of view, are data from the Atlantic West coast, and from the Mediterranean, as well as the Baltic Sea with ice probabilities. Both because of the different wind and wave climate ruling there and because of the practical needs for considerations about drift ice and icing due to spray. Additional sites outside Europe would also make out a relevant extension of the study, as many European entrepreneurs are active players in the now worldwide expansion of offshore wind energy.

In spite of these reservations, we have still chosen the UpWind design basis [1] as the basic illustrative data for this report, because it is a recent, large, comprehensive and accessible data base.

2.2 PARAMETERS FOR WIND AND WAVE SPECIFICATION

The core part of the design basis for an offshore wind farm consists of data for the wind and wave climate. The wind characteristics of a given site can be determined from multiyear measurements of wind speed and wind direction, preferably at several heights. Similar and simultaneous time series for the height and direction of the surface waves must be established.

The wind climate is characterised by

- mean speed
- wind direction
- wind shear
- turbulence standard deviation and turbulence intensity
- turbulence frequency spectrum
- extreme wind speed with 1 year and 50 year return period.

The wind measurements must be accompanied by measuring height, z , averaging time, often 10 min averages, sampling time, often 10min)

The wave climate is characterised by

- significant wave height, H_s (standard derived on basis of 3 hours data)
- peak period, T_p .
- wave direction
- frequency spectrum
- directional distribution
- misalignment (relative to the wind direction) distribution
- extreme value of H_s with T_p , and the derived heights, H_{Smax} , and H_{Sred} (with 1 and 50 year return period)

The multi-dimensional distribution function for these parameters must be considered to evaluate the design. Normally one can simplify the approach considerably, using physical and statistical knowledge. This is illustrated below, where we discuss the climate conditions as function of one parameter only, the wind speed. The basis for this approach is that the mean wind speed is the most important parameter to characterise both the wind turbulence and the wave field.

Additional information like water depth, tides, currents and temperature in air and water must be monitored at the measuring site too. This information is available in the data of the UpWind design basis [1] project along with information on marine growth and bottom soil features. Finally we note that the occurrence of water ice and icing, with associated loads, should be considered in relevant regions. This was not relevant, however, for the UpWind sites.

In the present report we will concentrate on the wind and wave information due to the focus of modelling and tests at the experimental facilities within the MaRINET project. Our approach is to seek for robust correlations between the wind and wave parameters important for the evaluation of both fatigue and extreme loads on offshore wind turbine structures. In order to do so, we start by summarising a simplified offshore climate driven by the wind speed in the next section.

2.3 ONE –PARAMETER CLIMATE BASED ON WIND SPEED.

In this section we seek to describe the design and load parameters for offshore wind turbines, both with respect to wind and other atmospheric parameters and with respect to the surface waves and other characteristic water parameters. A one-parameter approach is presented, where the wind speed is considered a free parameter and all the other quantities are described conditionally to the wind speed. In the following, the parameters of this description and their typical distributions are summarized.

2.3.1 Winds and other atmospheric parameters.

The distribution of the mean wind is normally taken as a Weibull distribution, in the medium to high wind interval as is illustrated in the Figure 2.3.1. The distribution can either be derived for each wind direction sector, or as the marginal distribution for all sectors. It has the following mathematical form:

$$(2.3.1) \quad f(V) = \frac{k}{A} \left(\frac{V}{A} \right)^{k-1} \exp \left(- \left(\frac{V}{A} \right)^k \right),$$

V being wind speed, and A and k being the scale parameter and shape parameter respectively. For the power and load estimates, the relevant height is the hub height, presently being 80-110 meter, which is the height interval used throughout the UpWind reference [1] and in the figures and tables here, copied from that report. By convention, however, wind climates are usually described at 10 m height. Conversion of the wind velocity between heights can be done with equation (2.3.2), or with equation (2.3.4), which is a power-law wind profile. Here we use (2.3.4) with, the power law exponent, $\alpha=0.14$, if nothing else is indicated, following the information in [1,2].

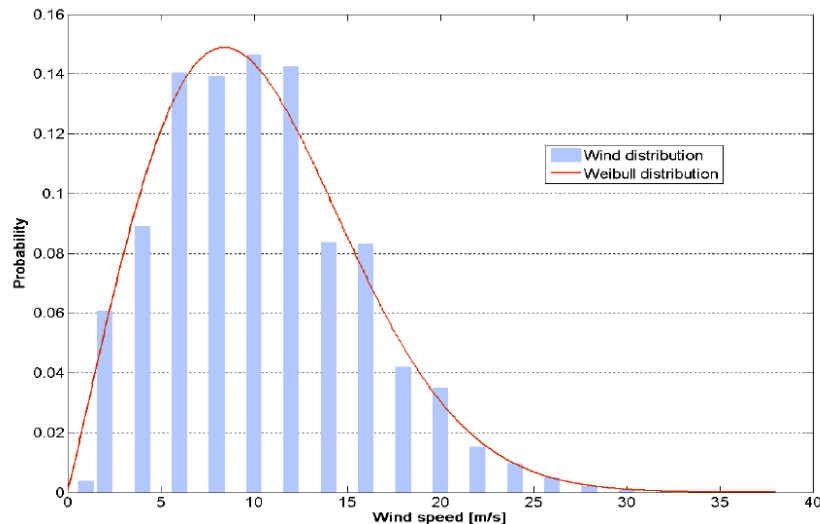


Figure 2.3.1 The 10 m wind distribution at hub-height from the IJmuiden site. From (1)

While the power-law profile is a commonly used approximation, the wind speed typically varies with height as given by the following profile expression:

$$(2.3.2) \quad V(z) = \frac{u_*}{\kappa} \left(\ln \left(\frac{z}{z_0} \right) - \psi(z, h, \Delta T) \right),$$

where z is the measuring height, u_* , the friction velocity, and z_0 the roughness length of the surface. Further Ψ is a correction function that becomes important if 1) z becomes significant relative to the height of the atmospheric boundary layer, h, or 2) the difference in temperature between the water and the air, ΔT , becomes significant. Together with the other parameters in the equation, ΔT describes the atmospheric thermal stability. Ψ is normally neglected over the ocean, but with the wind turbines reaching hub-heights larger than 100m, it may not be defensible anymore. As this subject is still under active research and is not yet included in the design standards, $\Psi=0$ is assumed throughout the present report.

The roughness height z_0 can be determined from Charnock's relation:



$$(2.3.3) \quad z_0 = C u_*^2 / g ,$$

where C is a coefficient between 0.01 and 0.015, dependent on the nearness of a coast (and to some extent also on wind and wave history), and g is the acceleration due to gravity. Over water, z_0 is a small quantity, of the order of 0.1-0.3 mm.

As an alternative to the log-law above one can use the so called power law profile given by

$$(2.3.4) \quad V(z) = V(z_{10})(z / z_{10})^\alpha ,$$

The power law coefficient α is taken as 0.14 in the UpWind design basis [1], which is also recommended in [2], but by comparison with the log-expression (2.3.2) it is seen that it will vary with z_0 and ΔT and also the z -interval used. This variation is neglected in most guideline and standard literature. Here it will show up together with the statistical scatter around the average behaviour. However, from both (2.3.2) and (2.3.4 with variable α), it is seen that the Weibull distribution must change both A and k with height, not only A , as would be the case with a constant α . Indeed closer studies show that typically k will increase from its value at 10m with height up to around 80m followed by a gradual decrease further up [16], showing a maximum variation of 0.5 across the boundary layer [16]. However, this is presently under research. In the present simplified description, the Weibull k parameter is therefore taken to be independent with height, consistent with the choice of a constant value of α .

In the EU-NORSEWIND project, the shear is measured directly from measuring stations in the North Sea and the Western Baltic typically around 100 meter above the sea surface. The measurements are based on both LIDARs and conventional profile instrumentation. The results show a fairly large scatter between stations and for each station. Typical distributions are shown in Figure 2.3.2. Estimates for the extreme shear values are given in the IEC 61400-1 design code [6].

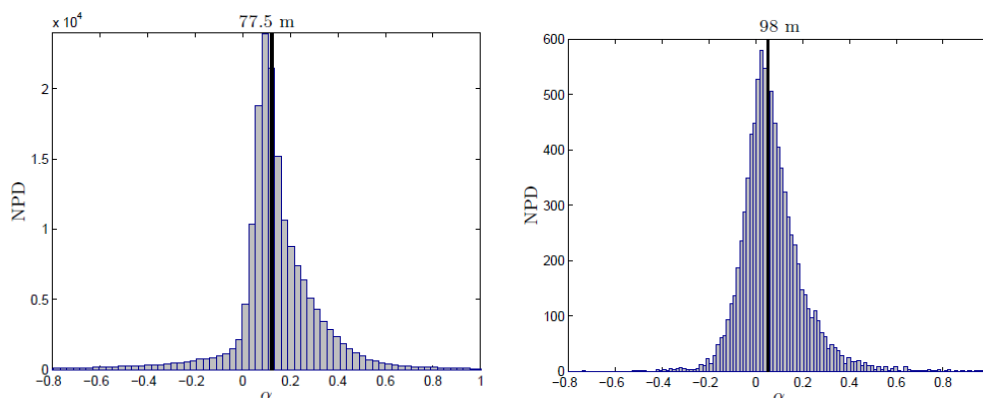


Figure 2.3.2. The shear power coefficient, α , from two North Sea sites, Greater Gabbard and Beatrice. From [13].

Using the expressions of (2.3.2) or (2.3.4) one can refer the 10-meter wind speed to hub-height, which is the speed normally used in connection with design studies. As seen from the figure a good deal of variability in the extrapolation must be expected due to the variability of the power coefficient. Equation (2.3.2) illustrates some of the sources to this variability, namely z_0 and the Ψ -function.

Additionally to the vertical profile of wind speed, the wind direction is logged with each recorded wind speed, and the direction will often be reported in terms of wind roses, with or without wind speed distributions as is exemplified

in Figure 2.3.3. The wind direction distribution, however, is not included in the simple one-parameter climate driven by the wind speed, which is the focus of the present section.

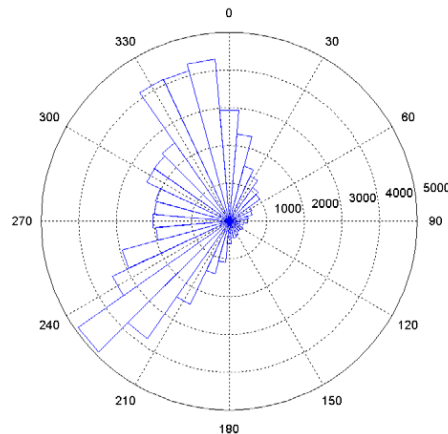


Figure 2.3.3. Wind Rose, wind direction distribution, with number of occurrences on the radial axis, from the IJmuiden data. From [1].

The turbulence intensity is given by $TI = \sigma_1 / V(z)$, where σ_1 is the standard deviation of the wind velocity turbulence. In design studies σ_1 is not simply derived as the mean value of a series of computed standard deviations, σ , around the mean wind. Rather it is the 90% quantile of the series of standard deviations [2]. Different fitting expressions are presented in the literature [2,6], where σ_1 is parameterised by the wind speed at hub-height. From [1] we present the most recent formulation over ocean conditions in equation (2.3.5) as well as in Figure 2.3.4 .

$$(2.3.5) \quad TI(V) = \frac{(15 + aV)}{(1 + a)V} I_{15}$$

Here the coefficient, a , is a coefficient around 5 and I_{15} is a reference turbulence intensity at 15 m/s, here taken as 0.15 or 0.14, see [6]. Note that the TI formulation in (2.3.5) does contain an explicit height variation.

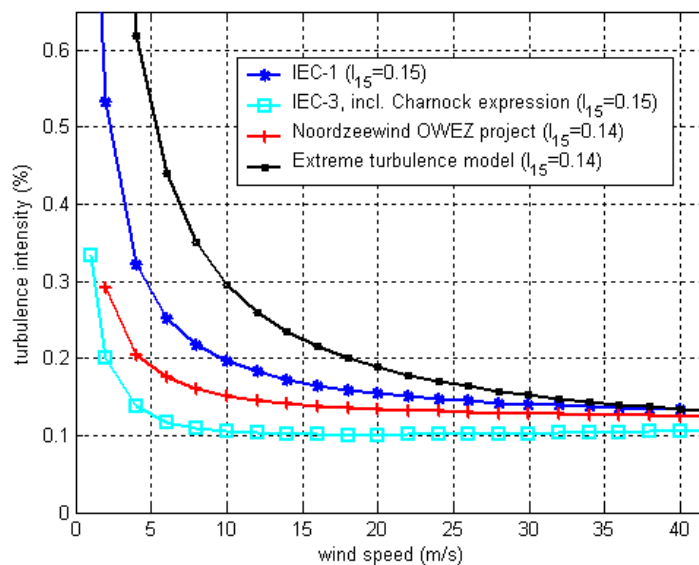


Figure 2.3.4. Turbulence Intensity at hub-height according UpWind, IEC (1,2,6). From [1].

For lower wind speeds, σ and σ_1 (the 90% quantile) do not decrease as fast as $V(z)$ for decreasing wind and TI increases for decreasing wind. For larger winds TI reaches a limit value, or does actually increase a little, due to an increasing z_0 with u_* as given by the Charnock relation (2.3.3).

Although we have here specified both the wind shear and the turbulence intensity as analytical functions of V , they will appear with statistical scatter around these expected values, when they are based on direct measurements. Further to the normal turbulence defined by (2.3.5) one can also specify an extreme turbulence intensity for certain load studies, see Figure 2.3.4.

Turbulence can be characterised by the frequency spectrum, $S(f)$, of the horizontal wind speed, scaling with the turbulence standard deviation, σ , and its spatial and temporal scales. The literature shows several forms that have a great deal of overlap as they all represent the same atmospheric physics, with similar combinations of data fitting and theory. Here we cite the Kaimal form as presented in [3]:

$$(2.3.6) \quad fS(f) = \sigma^2 \frac{4 \frac{Lf}{V_{10}}}{\left(1 + 6 \frac{Lf}{V_{10}}\right)^{5/3}},$$

where f is frequency (Hz), σ is the standard deviation of the turbulence and L is the characteristic turbulence length scale, taken as:

$$(2.3.7) \quad L = \begin{cases} 5.67z & \text{for } z < 60 \text{ m} \\ 340.2 & \text{for } z > 60 \text{ m} \end{cases}$$

The turbulence spectrum above describes the frequency distribution as well the wave number spectrum, because the atmospheric turbulence to a good approximation obey Taylors hypothesis of frozen turbulence, meaning that $f = V k_v / 2\pi$, where k_v is the wave number along the mean wind direction.

Figure 2.3.1 illustrates how the overall wind speed distributions are normally well approximated by Weibull distributions. However, these distributions are less satisfactory for extreme events. Here, it can be shown mathematically that the most common realistic extreme value distribution functions have high value tails that converge towards a Gumbel distribution, under the assumption of stationarity. From the observed wind records, one can now generate a distribution of maximum wind speeds over a given basic time that must be large enough for the maximum values to be independent of each other. Using the characteristics of the Gumbel distribution, one can next estimate extreme wind events that will happen in average over a certain period, denoted return period, e.g. once every year, 50 year or 100 year, even though the time series available are notably shorter than the larger of these return periods. According to the characteristics of the Gumbel distribution, the relation between the expected extreme wind and its return period can be found from:

$$(2.3.8) \quad V_T = \alpha - \beta \ln(-\ln(1 - T_0 / T)) \cong \alpha + \beta \ln(T / T_0) \equiv A + b \ln T,$$

where α and β are the most probable value and the standard deviation of the series of maximum values, respectively. Further, A and b are constants, derived from a fit to the maximum values plotted versus their estimated probability. Note that the middle approximation requires that $T \gg T_0$. Finally, A and b can be estimated from actual data series, as is illustrated in Figure 2.3.5.

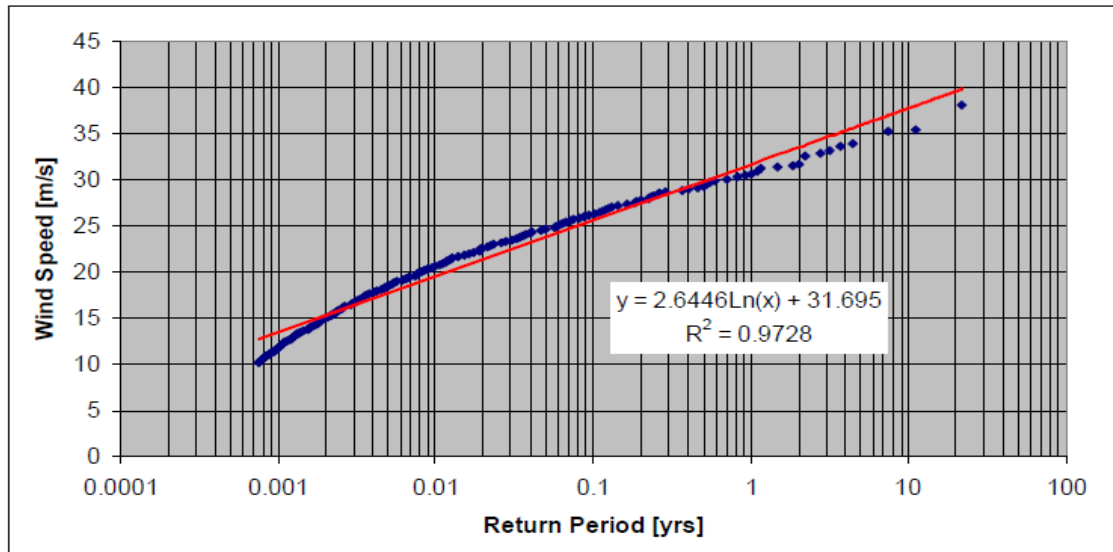


Figure 2.3.5. Extreme wind speed versus return period from UpWind IJmuiden data at hub-height. From [1].

From Figure 2.3.5 one can from the red line data fit determine the extreme wind with associated probability or return period, as presented in Table 2.3.1 [1]. Note, that there is some freedom for the line fit associated with eq. (2.3.8). While the red line appear to be based on the full data range, a closer fit to the extreme value observations could be obtained if the fit was performed closer to the tail of the distribution. This would yield somewhat smaller extreme winds.

| T_{return} [yr] | V_w [m/s] |
|-----------------------------|----------------|
| 1 | 31.70 |
| 5 | 35.95 |
| 10 | 37.78 |
| 50 | 42.04 |
| 100 | 43.87 |

Table 2.3.1. Summary of extreme wind versus return period at hub-height. IJmuiden data. From UpWind [1]

Obviously these kinds of extreme value estimations can be used on other measured parameters than the wind speeds, e.g. the shear or the turbulence intensity, but here one often prefer to work with distributions and conditional distributions, e.g. given certain winds speeds, as have been done for the extreme turbulence model in Figure 2.3.4. Specific combinations of wind- and wave parameters for extreme load cases are provided in the design code [6].

2.3.2 Waves and other oceanic parameters

When the wind blows over the water, surface waves will be generated. For reasonably homogeneous and stationary wind fields, the waves can generally be described by a fairly narrow band frequency spectrum that integrates to the variance of the wave field. Like the atmospheric turbulence the wave spectra show characteristic behaviour that have resulted in several analytical forms based on mixtures of theory and data fitting. The form presented here is extracted from [2]. The formulation starts with the Pierson-Moskowitz spectrum.

$$(2.3.9) \quad S_{PM}(f) = 0.3125 \cdot H_s^2 \cdot f_p^4 \cdot f^{-5} \cdot \exp\left(-1.25\left(\frac{f_p}{f}\right)^4\right),$$

where H_s is the significant wave height, f the frequency in Hz and f_p the peak frequency ($= 1/T_p$). The two parameters must be determined from other equations or from fitting to actual data. They depend on the duration and strength of the acting wind. Generally H_s increases and f_p decreases with fetch or duration of the wind.

The JONSWAP spectrum is formulated as a modification to the Pierson-Moskowitz spectrum and is more applicable to fetch limited situations and growing waves, as is found for most offshore wind turbine sites in the North Sea. It reads:

$$(2.3.10) \quad S_{JS}(f) = C(\gamma) \cdot S_{PM}(f) \cdot \gamma^\alpha,$$

where γ is denoted the peak enhancement parameter, α is a function of frequency and $C(\gamma)$ is a normalisation factor. The forms of the two spectra are illustrated in Figure 2.3.6.

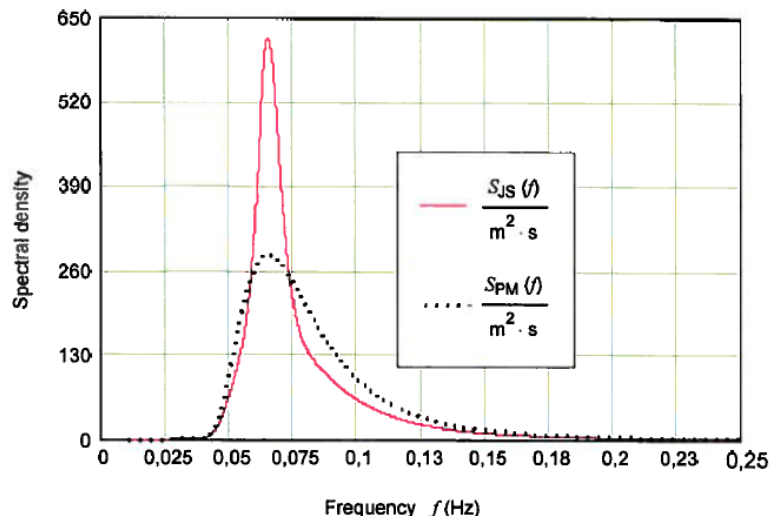


Figure 2.3.6. Sketch of the wave spectrum according to the Pierson-Moskowitz spectrum and according to the JONSWAP spectrum. From [9].

For $\gamma \rightarrow 1$ the Pierson-Moskowitz spectrum is recovered. Formulas for α and C are provided in [2]. The value of γ is often taken to be $\gamma = 3.3$ for storm waves and $\gamma = 1.0$ for fatigue calculations. It can also be estimated with basis in the spectral parameters [6] where H_s must be inserted in metres and T_p in seconds:

$$(2.3.11) \quad \gamma = \begin{cases} 5 & \text{for } \frac{T_p}{\sqrt{H_s}} \leq 3,6 \\ \exp\left(5,75 - 1,15 \frac{T_p}{\sqrt{H_s}}\right) & \text{for } 3,6 \leq \frac{T_p}{\sqrt{H_s}} \leq 5 \\ 1 & \text{for } \frac{T_p}{\sqrt{H_s}} > 5 \end{cases}$$

Even for a constant wind speed of wind direction θ_0 , all waves do not propagate along the wind direction, but in an angle interval around θ_0 . This is normally expressed by a directional wave spectrum [2,15], for example the 'cosine 2s spectrum'

$$(2.3.12) \quad S(f, \theta) = S(f) \cdot D(f, \theta), \text{ with } D(f, \theta) \approx \cos^s(\theta - \theta_0).$$

Here $D(f, \theta)$ normalises to 1 by integration over θ , and s is described by a complex function of f and the characteristics of the spectral function in (2.3.11), see [15].

Another reason for waves propagating in different directions from the local wind is that the wind is neither homogenous nor stationary, and waves generated at other times and places may propagate across the measuring site following the direction of the wind, when and where they were formed. They will typically appear at the lower frequency end of the locally generated $S_{js}(f)$ spectrum, because long waves dissipate slower than short waves. They are denoted swells, and will at some sites be significant.

As a final reason for the wave propagating direction to be off the wind direction, one must mention wave diffraction that can happen for the longer waves propagating onto lower water depth or due to interaction with a current. Just as for the wind one can establish a wave rose, summarising the climatic direction of the wave fields. Such one is illustrated in Figure 2.3.7.

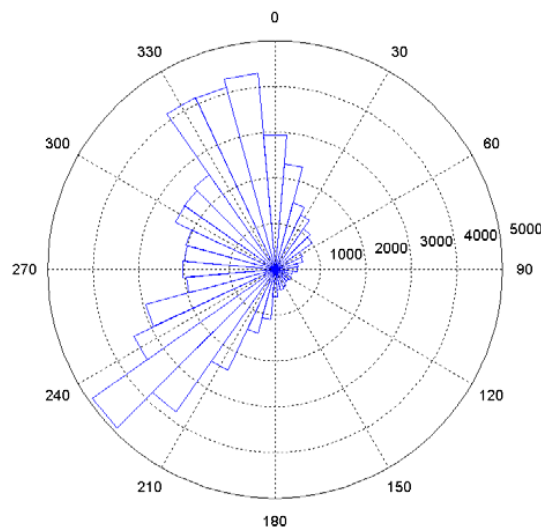


Figure 2.3.7. Wave rose. From [1]

As for winds, one could also from wave data derive climatic distributions of the characteristic wave parameters, H_s and f_p , but since wind speed is the dominating driver of the wave field, it is more useful to consider the wave parameters conditional to the wind parameters. Rather than a wave rose, as above, one focus on the directional difference between the wind and the wave direction, and rather than the climatic distribution of f_p and H_s one focuses on the relation of these parameters to the wind speed. The latter is typically done through a scatter matrix for the distribution of (H_s, T_p) conditional on the wind speed. Such matrices can be found in [1], while in the present report, we report only averaged values. Additionally, since the directional wave distribution is site specific in the present report, we shall use only unidirectional waves along the wind direction. However, for a real design one would need to consider the full scatter diagrams of wind- and wave direction. In Table 2.3.2 we illustrate the combined marginal distribution of wind and wave direction for all wind speeds, taken from one of the UpWind sites [1]. Since the wave direction distribution as stated is site specific, we have not tried to merge the different Tables of [1] from the different UpWind sites.

| All windspeeds | | Wave direction | | | | | | | | | | | | |
|----------------|-----|----------------|---------|---------|---------|---------|---------|---------|---------|---------|---------|---------|---------|---------|
| | | 000° | 030° | 060° | 090° | 120° | 150° | 180° | 210° | 240° | 270° | 300° | | 330° |
| Wind direction | | N | NNE | ENE | E | ESE | SSE | S | SSW | WSW | W | WNW | NNW | |
| 000° | N | 0,03839 | 0,00504 | 0,00093 | 0,00028 | 0,00011 | 0,00025 | 0,00058 | 0,00089 | 0,00070 | 0,00095 | 0,00188 | 0,01143 | 0,06143 |
| 030° | NNE | 0,02819 | 0,01846 | 0,00422 | 0,00081 | 0,00028 | 0,00044 | 0,00065 | 0,00073 | 0,00054 | 0,00042 | 0,00103 | 0,00408 | 0,05984 |
| 060° | ENE | 0,01299 | 0,02210 | 0,01739 | 0,00319 | 0,00081 | 0,00065 | 0,00067 | 0,00067 | 0,00050 | 0,00044 | 0,00073 | 0,00201 | 0,06214 |
| 090° | E | 0,00779 | 0,01036 | 0,02462 | 0,01454 | 0,00359 | 0,00160 | 0,00115 | 0,00079 | 0,00048 | 0,00045 | 0,00068 | 0,00210 | 0,06818 |
| 120° | ESE | 0,00571 | 0,00510 | 0,00821 | 0,01199 | 0,01052 | 0,00554 | 0,00314 | 0,00138 | 0,00087 | 0,00050 | 0,00079 | 0,00193 | 0,05569 |
| 150° | SSE | 0,00534 | 0,00336 | 0,00322 | 0,00414 | 0,00607 | 0,01034 | 0,01384 | 0,00443 | 0,00110 | 0,00107 | 0,00165 | 0,00249 | 0,05706 |
| 180° | S | 0,00675 | 0,00263 | 0,00198 | 0,00210 | 0,00213 | 0,00470 | 0,02792 | 0,02117 | 0,00436 | 0,00252 | 0,00275 | 0,00453 | 0,08353 |
| 210° | SSW | 0,00639 | 0,00229 | 0,00151 | 0,00098 | 0,00103 | 0,00208 | 0,01790 | 0,06882 | 0,01322 | 0,00633 | 0,00583 | 0,00762 | 0,13401 |
| 240° | WSW | 0,00652 | 0,00196 | 0,00095 | 0,00070 | 0,00058 | 0,00109 | 0,00621 | 0,04693 | 0,03393 | 0,01756 | 0,01120 | 0,01034 | 0,13796 |
| 270° | W | 0,00778 | 0,00137 | 0,00081 | 0,00022 | 0,00033 | 0,00044 | 0,00218 | 0,01352 | 0,01989 | 0,02697 | 0,02750 | 0,01618 | 0,11718 |
| 300° | WNW | 0,01224 | 0,00148 | 0,00042 | 0,00014 | 0,00023 | 0,00030 | 0,00107 | 0,00445 | 0,00554 | 0,00885 | 0,02083 | 0,03029 | 0,08583 |
| 330° | NNW | 0,02870 | 0,00180 | 0,00047 | 0,00019 | 0,00028 | 0,00025 | 0,00107 | 0,00182 | 0,00143 | 0,00216 | 0,00625 | 0,03274 | 0,07717 |
| | | 0,16678 | 0,07596 | 0,06472 | 0,03928 | 0,02595 | 0,02767 | 0,07639 | 0,16560 | 0,08257 | 0,06822 | 0,08113 | 0,12573 | 1,00000 |

Percentage of time [%]

| |
|---------------------------|
| 90° + from wind direction |
| 90° - from wind direction |

Table 2.3.2. Distribution of simultaneous propagation directions for wind and waves, taken from the K13 site in UpWind. Taken from [1].

2.3.3 Lumped wind-wave climate for fatigue calculation

While the full wind-wave climate at a site is a multi-dimensional parameter space with a multi-dimensional statistical distribution function, it can be practically expressed in terms of a one-parameter climate conditional to the wind speed. In this approach, central values of all other parameters are determined by suitable averaging through the parameter space. The overall purpose of such a simpler climate description is to simplify the fatigue calculations for the structure. Therefore, the averaging of the climate parameters is done with respect to fatigue contribution and not simply with respect to probability of occurrence. An example of such a lumped wind-wave climate is given in Table 2.3.3 which shows the wave and wind parameters as function of mean wind speed at hub height together with the frequency of occurrence for each wind speed bin. The statistics in the table are lumped according to the method of Kühn [1, 43]. Two turbulence intensity values are shown, namely those associated with the normal and extreme turbulence models, see [1]. It should be emphasized that the estimates of turbulence intensity are derived from the normal turbulence model used also in Figure 2.3.4 and in (2.3.4), based on assumptions about the distribution of TI for a given wind speed.

The two γ -values of 1.0 and 3.3 are quite usual, and we shall return to this in section 2.4. Finally, we point out that H_s and T_p values are weighted values for a given wind speed. Individual values will scatter statistical around these averages.

It should be mentioned that the fatigue-weighting of the wave data cited here was done for bottom fixed wind turbines. Hence, for a floating wind turbine, the weighting is likely to be different and might thus lead to other weighted values of H_s and T_p . Currently an extensive study is conducted by NREL, University of Massachusetts, and University of Stuttgart to address this question. A large set of aero-elastic simulations (1-2 million of 10min duration) is made and will be used to establish a recommendation for simplifying load cases for extreme and fatigue calculations for floating wind turbines. First results from the study will be presented at OMAE 2013: "L. Haid, G. Stewart, Jason Jonkman, Matthew Lackner, Denis Matha, Amy Robertson 'Simulation-Length Requirements in the Loads Analysis of Offshore Floating Wind Turbines'".

| V [ms] | TI [%] | | Hs [m] | Tp [m] | Peakness [-] | | f [%] | occ./year [hrs] |
|-----------|-----------|---------|-----------|-----------|-----------------|---------|----------|--------------------|
| | normal | extreme | | | Fatigue | Extreme | | |
| 2 | 29,2 | 99,3 | 1,07 | 6,03 | 1 | 3,3 | 0,06071 | 531,8 |
| 4 | 20,4 | 53,1 | 1,1 | 5,88 | 1 | 3,3 | 0,08911 | 780,6 |
| 6 | 17,5 | 37,1 | 1,18 | 5,76 | 1 | 3,3 | 0,14048 | 1230,6 |
| 8 | 16 | 30 | 1,31 | 5,67 | 1 | 3,3 | 0,13923 | 1219,7 |
| 10 | 15,2 | 25,4 | 1,48 | 5,74 | 1 | 3,3 | 0,14654 | 1283,7 |
| 12 | 14,6 | 22,3 | 1,7 | 5,88 | 1 | 3,3 | 0,14272 | 1250,2 |
| 14 | 14,2 | 20,1 | 1,91 | 6,07 | 1 | 3,3 | 0,08381 | 734,2 |
| 16 | 13,9 | 18,5 | 2,19 | 6,37 | 1 | 3,3 | 0,08316 | 728,5 |
| 18 | 13,6 | 17,2 | 2,47 | 6,71 | 1 | 3,3 | 0,04186 | 366,7 |
| 20 | 13,4 | 16,1 | 2,76 | 6,99 | 1 | 3,3 | 0,03480 | 304,8 |
| 22 | 13,3 | 15,3 | 3,09 | 7,4 | 1 | 3,3 | 0,01534 | 134,4 |
| 24 | 13,1 | 14,6 | 3,42 | 7,8 | 1 | 3,3 | 0,00974 | 85,3 |
| 26 | 12 | 14 | 3,76 | 8,14 | 1 | 3,3 | 0,00510 | 44,7 |
| 28 | 11,9 | 13,5 | 4,17 | 8,49 | 1 | 3,3 | 0,00202 | 17,7 |
| 30 | 11,8 | 13,1 | 4,46 | 8,86 | 1 | 3,3 | 0,00096 | 8,4 |
| 32 | 11,8 | 12,7 | 4,79 | 9,12 | 1 | 3,3 | 0,00050 | 4,4 |
| 34-42 | 11,7 | 12,3 | 4,9 | 9,43 | 1 | 3,3 | 0,00019 | 1,6 |

Table 2.3.3. Lumped wind-wave climate conditional to wind speed at hub height (here 85 meter above mean sea level). The table provides turbulence intensities, significant wave height, period of the peak frequency, and peaked-ness for the wave spectrum, probability of occurrence, or correspondingly duration of occurrence per year. Data are from the K13 site from the UpWind project. Taken from [1].

2.3.4 Extreme values for wave climate

The lumped statistics of data in the table above is very suitable for fatigue load studies. For the extreme loads one must use the extreme values of both winds and wave heights as estimated by the Gumbel statistics in the text above, corresponding to a 1 year and 50 year return period. This is illustrated in figure 2.3.8, also taken from the K13 site in the UpWind report [1].

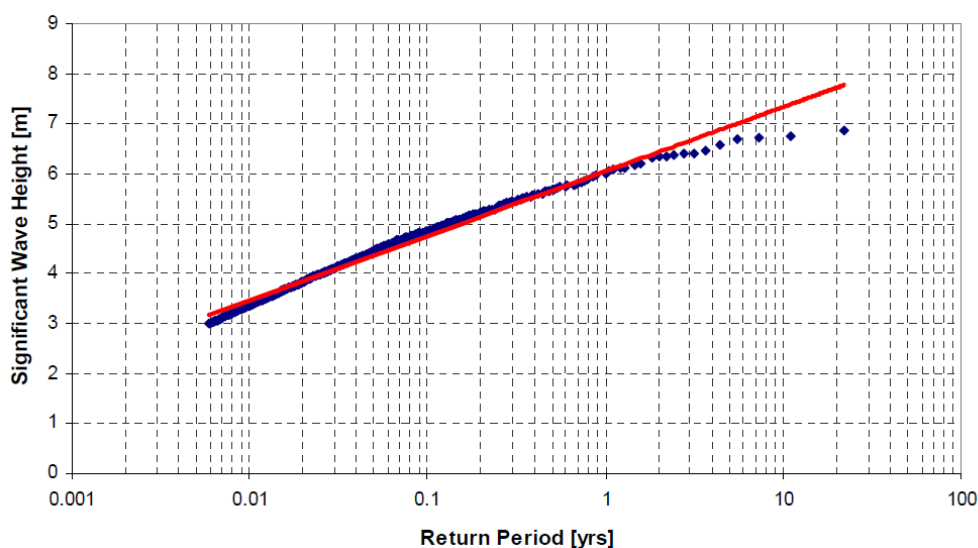


Figure 2.3.8. Extreme H_s versus return period by the Gumbel method for the K13 shallow depth site of UpWind. From [1].

From Figure (2.3.8), we can summarise the extreme waves as function of the return period:

| T_{return} [yr] | H_s [m] | T_p [s] | H_{max} [m] |
|----------------------|--------------|--------------|------------------|
| 1 | 6.05 | 10.12 | 11.25 |
| 5 | 6.95 | 10.54 | 12.93 |
| 10 | 7.34 | 10.69 | 13.65 |
| 50 | 8.24 | 10.97 | 15.33 |
| 100 | 8.63 | 11.05 | 16.05 |

Table 2.3.4. Extreme significant wave heights as derived from the Gumbel corresponding to the UpWind K13 shallow depth site. From [1].

The H_s - value is taken directly from the Gumbel fit method of the Figure 2.3.8. Similar remarks as for Figure 2.3.5 on the range of line-fitting and the implication for the extreme values of Table 2.3.4 apply. H_{max} is based on that H_s is derived from an average over 3 hours and that the waves are Rayleigh distributed, giving rise to a maximum value being ~ 1.86 times H_s [2]. The peak period corresponding to the extreme wind speeds must be bounded by the following formula criterion, [2]:

$$(2.3.12) \quad 11.1\sqrt{H_s(U)/g} \leq T \leq 14.3\sqrt{H_s(U)/g},$$

where one should select the peak period that results in the strongest loads.

2.4 STANDARD OFFSHORE CONDITIONS FOR TESTING AND MODELLING

In this section we extract a set of offshore standard conditions for test and modelling. The extraction is made from data of the UpWind design basis and from the Beatrice and Södra Midsjöbank sites.

2.4.1 Wind climate parameters in the extended North Sea and Baltic Sea

The wind conditions over the extended North Sea and Baltic Sea is illustrated in Figure 2.4.1 and 2.4.2 taken from the EU-NORTHWIND reporting [13, 14] on the marine winds of NW Europe. Figure 2.4.1 shows the mesoscale modelling result of the average 100 meter wind speed 2006-11, while the four plots of Figure 2.4.2 depicts the marine wind climate at 10 meter height measured by radar from 10 year satellite measurements [14]. The figures illustrate the variability of wind parameters in the extended North Sea and Baltic Sea.

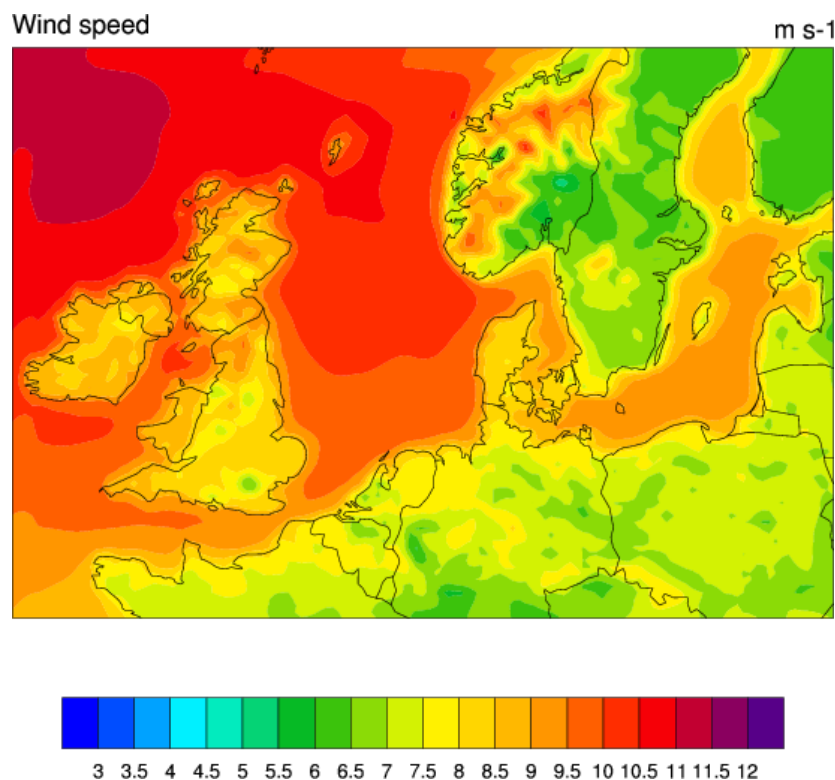


Figure 2.4.1. The variation of the 100 m mean wind across the NorthWestern European waters, as modelled by mesoscale modelling, Norsewind. From [13].

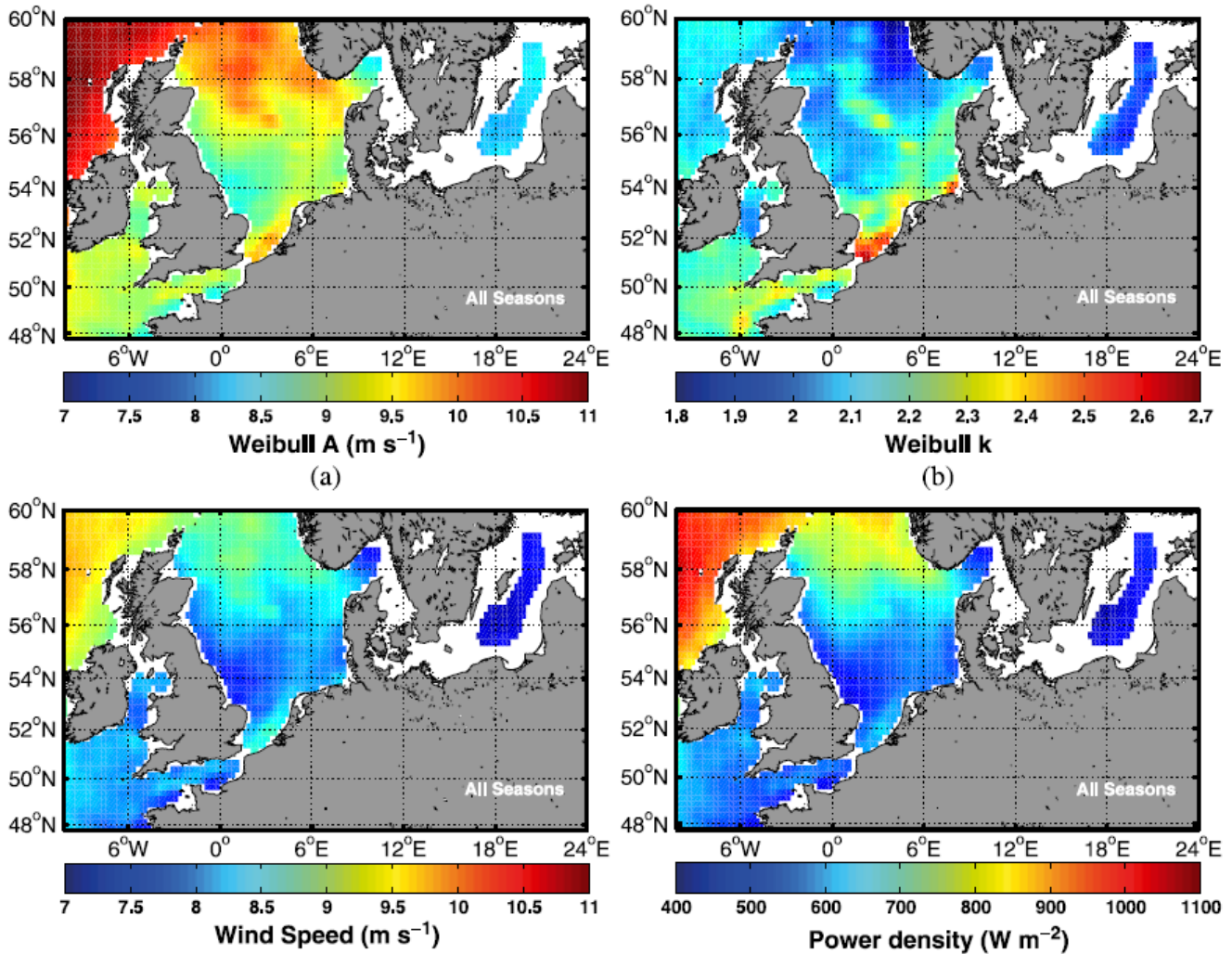


Figure 2.4.2. The 10 meter marine wind climate across the North Western European seas. The white areas correspond to lack of data, mainly due to precipitation. From [14].

The figures indicate that one should expect a fairly gradual change in the wind characteristic of the North Western European waters, with exception of the quite close to coastal areas. At 10 m above the surface, a typical Weibull A parameter is seen to be about 9 m/s, with a k-value about 2. The A and k-value seems of the order of the ones derived from the 10m distributions in Figure 2.4.3 and presented in Table 2.4.1.

2.4.2 Wind and wave climate for five specific sites

We now compare the wind and wave climate parameters for five sites, namely the three sites of the UpWind design basis, the Beatrice site and Södra Midsjöbanken. The UpWind data are extracted from [1], while the Beatrice and Södra Midsjöbanken results are taken from [10,11]. It should be noted that the wave data from Södra Midsjöbanken are not based on measurements but have been calculated with closed-form wave growth models.

A first summary is provided in Table 2.4.3 which lists the Weibull wind distribution parameters, the extreme (1,50)-year wind speed and significant wave heights, the water depth and the lumped wave climate parameters for $V_{10}=20\text{m/s}$. Given the difference in geographical location, the similarity between the wind and wave parameters is quite remarkable. Further, the 10 meter A and k values of the table compare quite well with the satellite data of Figure 2.4.2.

| Site | A ₁₀ | K | H _s V ₁₀ = 20m/s | T _p , V ₁₀ = 20m/s | V ₅₀ m/s | V ₁ m/s | H _{s,50} m | H _{s,1} M | Depth m |
|-----------------------|-----------------|-----|---|---|------------------------|-----------------------|------------------------|-----------------------|------------|
| IJmuiden | 7.9 | 2.1 | 4.2 | 8.7 | 31.5 | 23.8 | 7.6 | 5.7 | 21 |
| K13 shallow | 9.3 | 2.0 | 3.5 | 8.0 | 34.1 | 25.9 | 8.2 | 6.1 | 25 |
| K13 Deep | 9,3 | 2.1 | 3.5 | 8.0 | 34.1 | 25.9 | 9.4 | 7.1 | "50" |
| Beatrice | 8,7 | 1,9 | 3.8 | 6.5 | 38.5 | - | - | - | 44 |
| Södra Midsjöbanken | 8,2 | 2.1 | "3.3" | "7.5" | 35.2 | - | - | - | 15 |

Table 2.4.1 Summary of parameters from the 5 sites considered. Note that the wave parameters from Södra Midsjöbanken are modelled and not based on measurements. On the K13 Deep site, the depth is indicated by "50", because of the way the K13 Deep data set is made, see section 2.1. The H_s and T_p data from Södra Midsjöbanken are marked with " " also, because they are based on wave growth models not data. At Beatrice and Södra Midsjöbanken no other extreme values than the 50-year wind speed were determined.

Next, two tables of lumped wind-wave climates are provided in Table 2.4.2 and 2.4.3, pertaining to the IJmuiden shallow water site and the K13 shallow water site. The similar table for the K13 deep water site (not shown here) is identical to the one of the K13 shallow water side except for 1) the probabilities, which are associated with the difference in the Weibull parameters for the wind speed distribution at the two sites; and 2) the extreme wave data, which are not listed in these tables.

| V [ms] | TI [%] | | H _s [m] | T _p [m] | Peakness [-] | f [%] | occ./year [hrs] |
|-----------|-----------|---------|-----------------------|-----------------------|-----------------|----------|--------------------|
| | normal | extreme | | | | | |
| 2 | 29,2 | 99,3 | 1,07 | 6,03 | 3,3 | 0,06239 | 546,5 |
| 4 | 20,4 | 53,1 | 1,1 | 5,88 | 3,3 | 0,11898 | 1042,2 |
| 6 | 17,5 | 37,1 | 1,18 | 5,76 | 3,3 | 0,15494 | 1357,3 |
| 8 | 16 | 30 | 1,31 | 5,67 | 3,3 | 0,16479 | 1443,5 |
| 10 | 15,2 | 25,4 | 1,48 | 5,74 | 3,3 | 0,15130 | 1325,4 |
| 12 | 14,6 | 22,3 | 1,7 | 5,88 | 3,3 | 0,12285 | 1076,2 |
| 14 | 14,2 | 20,1 | 1,91 | 6,07 | 3,3 | 0,08932 | 782,5 |
| 16 | 13,9 | 18,5 | 2,19 | 6,37 | 3,3 | 0,05858 | 513,1 |
| 18 | 13,6 | 17,2 | 2,47 | 6,71 | 3,3 | 0,03480 | 304,8 |
| 20 | 13,4 | 16,1 | 2,76 | 6,99 | 3,3 | 0,01878 | 164,5 |
| 22 | 13,3 | 15,3 | 3,09 | 7,4 | 3,3 | 0,00922 | 80,8 |
| 24 | 13,1 | 14,6 | 3,42 | 7,8 | 3,3 | 0,00413 | 36,2 |
| 26 | 12 | 14 | 3,76 | 8,14 | 3,3 | 0,00168 | 14,8 |
| 28 | 11,9 | 13,5 | 4,17 | 8,49 | 3,3 | 0,00063 | 5,5 |
| 30 | 11,8 | 13,1 | 4,46 | 8,86 | 3,3 | 0,00021 | 1,9 |
| 32 | 11,8 | 12,7 | 4,79 | 9,12 | 3,3 | 0,00007 | 0,6 |
| 34-42 | 11,7 | 12,3 | 4,9 | 9,43 | 3,3 | 0,00003 | 0,2 |

Table 2.4.2 Lumped statistics from the IJmuiden site. The wind speed refers to the hub height (83.9 m). From [1].

| V [ms] | TI [%] | | Hs [m] | Tp [m] | Peakness [-] | | f [%] | occ./year [hrs] |
|-----------|-----------|---------|-----------|-----------|-----------------|---------|----------|--------------------|
| | normal | extreme | | | Fatigue | Extreme | | |
| 2 | 29,2 | 99,3 | 1,07 | 6,03 | 1 | 3,3 | 0,05395 | 472,6 |
| 4 | 20,4 | 53,1 | 1,1 | 5,88 | 1 | 3,3 | 0,10177 | 891,5 |
| 6 | 17,5 | 37,1 | 1,18 | 5,76 | 1 | 3,3 | 0,13431 | 1176,6 |
| 8 | 16 | 30 | 1,31 | 5,67 | 1 | 3,3 | 0,14768 | 1293,7 |
| 10 | 15,2 | 25,4 | 1,48 | 5,74 | 1 | 3,3 | 0,14288 | 1251,6 |
| 12 | 14,6 | 22,3 | 1,7 | 5,88 | 1 | 3,3 | 0,12459 | 1091,4 |
| 14 | 14,2 | 20,1 | 1,91 | 6,07 | 1 | 3,3 | 0,09917 | 868,7 |
| 16 | 13,9 | 18,5 | 2,19 | 6,37 | 1 | 3,3 | 0,07259 | 635,9 |
| 18 | 13,6 | 17,2 | 2,47 | 6,71 | 1 | 3,3 | 0,04910 | 430,1 |
| 20 | 13,4 | 16,1 | 2,76 | 6,99 | 1 | 3,3 | 0,03079 | 269,7 |
| 22 | 13,3 | 15,3 | 3,09 | 7,4 | 1 | 3,3 | 0,01793 | 157,1 |
| 24 | 13,1 | 14,6 | 3,42 | 7,8 | 1 | 3,3 | 0,00972 | 85,1 |
| 26 | 12 | 14 | 3,76 | 8,14 | 1 | 3,3 | 0,00491 | 43,0 |
| 28 | 11,9 | 13,5 | 4,17 | 8,49 | 1 | 3,3 | 0,00231 | 20,2 |
| 30 | 11,8 | 13,1 | 4,46 | 8,86 | 1 | 3,3 | 0,00101 | 8,9 |
| 32 | 11,8 | 12,7 | 4,79 | 9,12 | 1 | 3,3 | 0,00042 | 3,6 |
| 34-42 | 11,7 | 12,3 | 4,9 | 9,43 | 1 | 3,3 | 0,00024 | 2,1 |

Table 2.4.3 Lumped statistics from the K13 shallow site. The wind speed refers to the hub height (85.2 m). From [1].

The similarity and differences between the different sites are now analysed in terms of graphical comparison. Figure 2.4.3 shows the wind distributions together with raw data and the fitted Weibull distributions. The Weibull parameters are those of Table 2.4.1. In general a reasonable match to the Weibull curve is observed. Further, as is also reflected by the similarity of the Weibull parameters in Table 2.4.1, the wind distributions from the different sites are fairly similar.

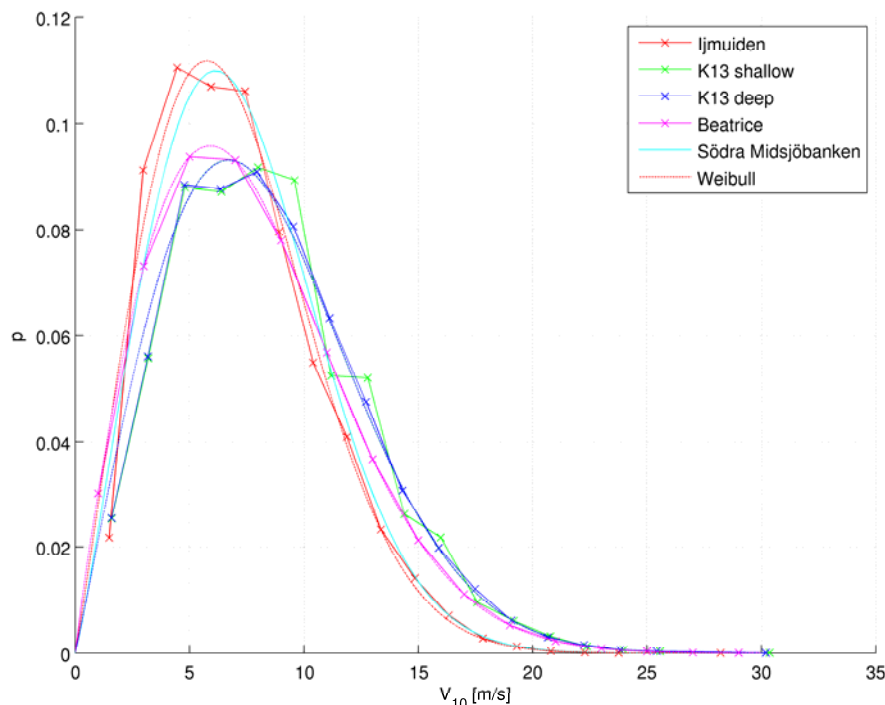


Figure 2.4.3 The 10 m wind speed distribution at the 5 sites considered, compared to each other and an analytical Weibull function.

The turbulence intensity at hub height is compared in Figure 2.4.4. The turbulence intensity for the three UpWind sites were based on the formula in (2.3.5) rather than on measurements and are therefore in good agreement. The Beatrice values are smaller. The value of (2.3.5) for $a=5$ m/s and $I_{15}=0.14$ are shown on the figure as well.

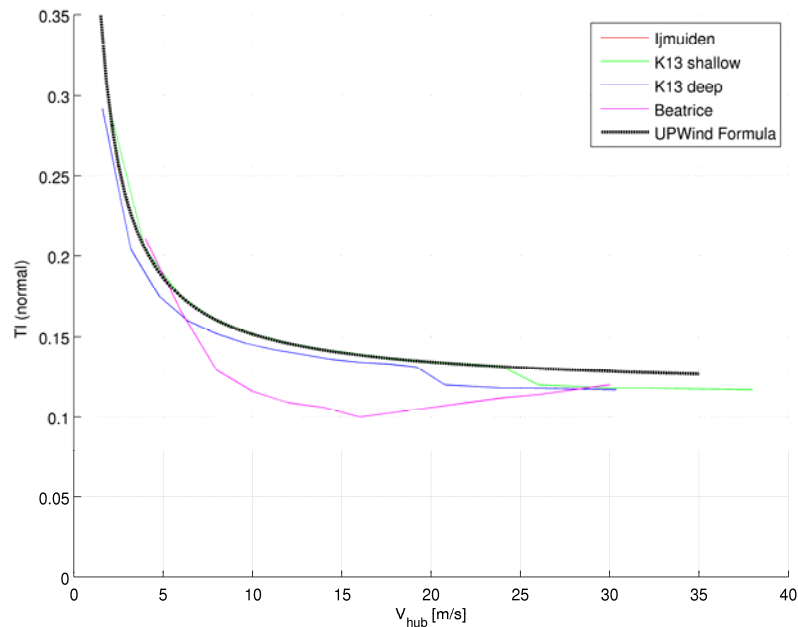


Figure 2.4.4. Normal turbulence intensity versus wind speed at the hub height from 4 of the sites considered. The black curve is the normal turbulence formula from [1] given in (2.3.5), which is the basis for the TI estimates from the UpWind sites. The Beatrice TI is determined from TI values over the North Sea extrapolated by use of (2.3.3). No independent TI was estimated at the fifth site.

The dependence of significant wave height H_s to wind speed is compared in Figure 2.4.5. The curves for the four sites are seen to be very similar. This suggests that a generic relation might exist, although it should be noted that the values are based on fatigue-lumped H_s values which might thus induce some dependence to structural parameters. Nevertheless, an analytical function was fitted to the data. It was found that the curve

$$(2.4.1) \quad H_s/H_0 = 1 + 2.6 (V/V_0)^3 / (1 + (V/V_0)^2) \quad H_0 = 1 \text{ m} , V_0 = 13 \text{ m/s}$$

provides a reasonable fit to the data.

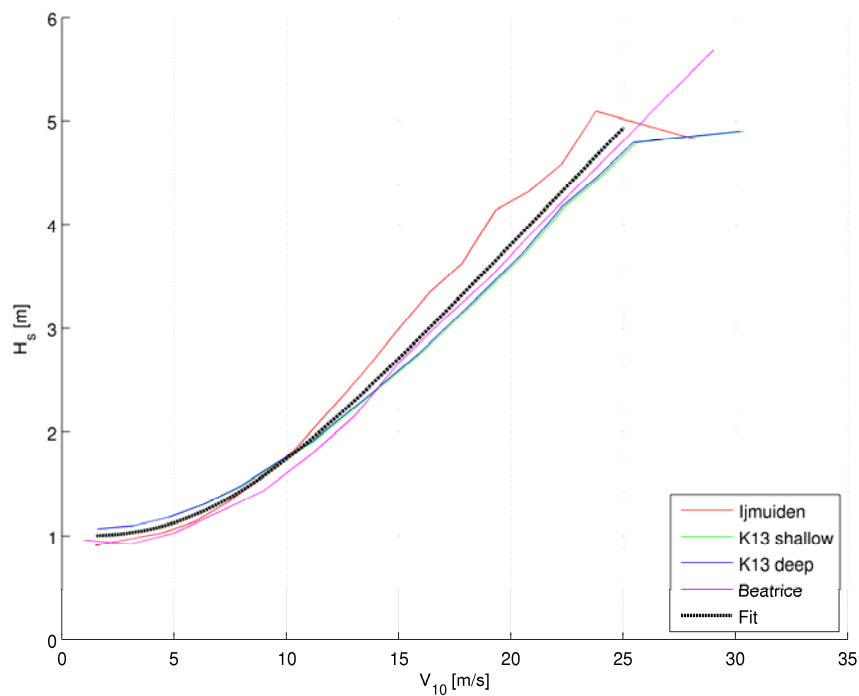


Figure 2.4.5. H_s versus the 10 meter wind speed for the 4 sites considered with wave measurements. The H_s values for the fifth site were estimated from wave models only and are not shown here. The fit is defined as $H_s/H_0 = 1 + 2.6 (V/V_0)^3 / (1 + (V/V_0)^2)$, with $H_0 = 1\text{ m}$ and $V_0 = 13\text{ m/s}$.

The correlation of peak period and significant wave height is shown in Figure 2.4.6. For the UpWind data, the two curves of K13 shallow and K13 deep are identical. Further, the correlation for IJmuiden is seen to be quite similar to that from K13. The correlation from Beatrice, however, is seen to have substantially smaller values of T_p than the UpWind sites. This may be due to a difference in the applied method for fatigue-based lumping, as the lumped T_p values of Beatrice were weighted with $1/T_p$ to reflect the number of stress-cycles associated with a given period. On the figure, the curves

$$(2.4.2) \quad T_p = a \sqrt{H_s/g}$$

with $a=11.1$ and $a=14.3$ have also been included. This reflects the requirement of (2.3.12). It is seen that the data is within these bounds, except for the Beatrice data which is very close and sometimes smaller (T_p -wise) than the limit associated with $a=11.1$.

All three curves show a peculiar upward turn for small H_s values. This behaviour is not reflected in the generic curves associated with (2.4.2) and may thus either be site-specific or simply a consequence of the fatigue-lumping.

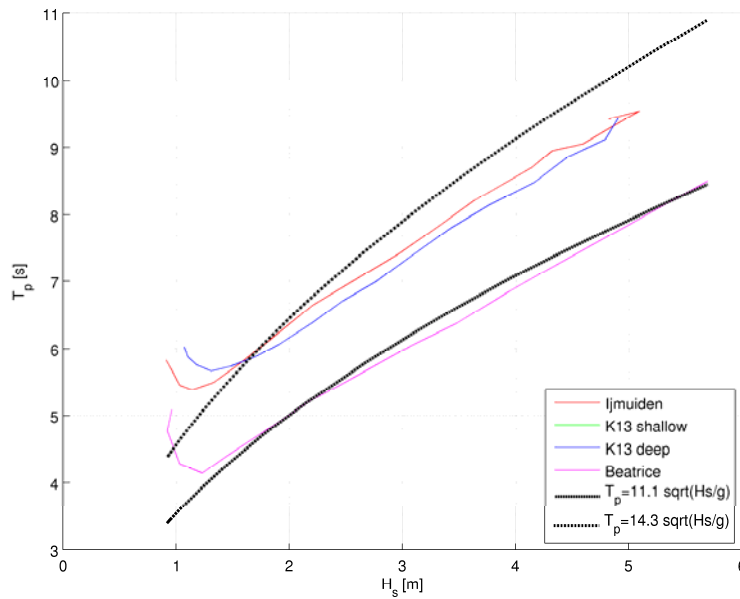


Figure 2.4.6. T_p versus H_s , estimated from data at the four sites considered. For the UpWind sites (2), the data are tabulated in section 2.3. The Beatrice curve is from [10] and is on the lower bound, which may reflect the nearness of the coast at this site. The two analytical curves reflect bounds for T_p in (2.3.12).

The JONSWAP peak enhancement parameter, γ , is determined from (2.3.11) and depicted in figure 2.4.7. It is seen that the UpWind sea states show a general increase in γ for increasing wind speed, towards a maximum value of approximately 2.5. The Beatrice values grow readily to a value of $\gamma=5$, which is very large. This may be explained by the relatively small T_p values, which again might be a consequence of the fatigue-lumping method rather than the actual sites wave climate.

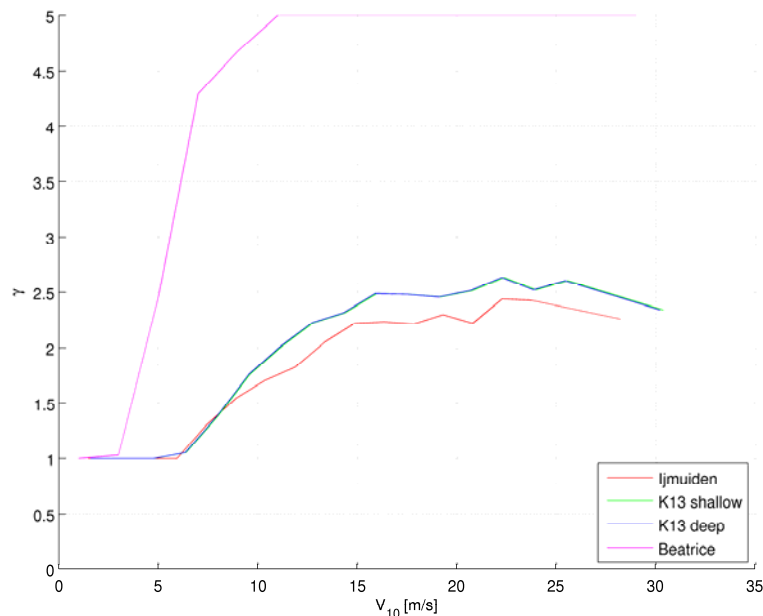


Figure 2.4.7. The peak factor γ versus the 10 meter wind speed for the 4 sites considered. The high values from Beatrice reflect the relatively low T_p values for this site, see Figure 2.4.4.

2.4.3 Recommendation

On the basis of the analysis and comparisons of the wind-wave climates at the five selected sites, the following approach for the generation of generic wind-wave climates for model test purposes and generic numerical computation is recommended:

1. The wind distribution is chosen as a Weibull distribution with parameters similar to the ones in Figure 2.4.3 / Table 2.4.1. The wind speeds are extrapolated to hub height by use of the power law profile given in equation (2.3.4). A power law coefficient of $\alpha= 0.14$ is applied, consistent with IEC 1604-3 [2]. When choosing the Weibull parameters, one should consider both the geographic variation, illustrated in this section, and the uncertainty associated with their height extrapolation, discussed in section 2.3.
2. With basis in the chosen wind distribution, a number of wind speed bins with associated probability are determined.
3. For each wind speed, the associated normal turbulence intensity is determined from Figure 2.4.4.
4. For each wind speed, a H_s value is determined from Figure 2.4.5 or the fitted formula (2.4.1).
5. The associated T_p value is estimated from Figure 2.4.6. The data shows quite some scatter but falls within the bounds determined from (2.3.12).
6. The JONSWAP peak enhancement factor γ is chosen as $\gamma=1.0$ for fatigue studies or $\gamma=3.3$ for ultimate load cases. Alternatively, one can determine γ from equation (2.3.11).
7. Extreme values of wind speed and wave height are chosen from Table 2.4.1. A choice consistent with the chosen Weibull distribution is recommended.

Hereby a lumped wind-wave climate is established along with extreme values for wind speed and wave height. The climates are not intended as a replacement of any real data for a specific site. But with no data available the procedure can serve to exemplify the relevant parameters and their correlation with wind speed.

3 SCALING OF WIND AND WAVE CONDITIONS FOR PHYSICAL MODEL TEST

In this section, we review the relevant scaling considerations for offshore wind turbines that are subject to simultaneous loads from waves and wind. A recent study for a floating wind turbine is reviewed too. Next, the suggested scaling methodology is derived and a scaling method for structural parameters and wind/wave climate parameters are devised. The scaling method is applied to a simple numerical model for a floating TLP (Tension Leg Platform) wind turbine, subjected to an external climate of section 2.4. It is demonstrated that a perfect reproduction of structural response at model scale can be achieved, provided that the structural loads are reproduced correctly. This requirement implies a re-design of the blades due to the smaller Reynolds number at model scale and assumes insensitivity of the hydrodynamic load coefficients to the hydrodynamic Reynolds number. The limitations of the scaling procedure are discussed.

3.1 REVIEW OF EXISTING SCALING STUDIES AND RELEVANT NONDIMENSIONAL NUMBERS

Although offshore wind turbines are predominantly bottom fixed, most of the existing studies of simultaneous wind and wave loads in offshore wind energy are concerned with floating wind turbines. This is attributed to the larger response of the support structure compared to bottom fixed structures.

Until now, only little material has been published regarding FOWT (Floating Offshore Wind Turbine) scale model testing. The scale testing efforts related to prototypes of FOWT (e.g. Statoil's Hywind prototype or EDP's WindFloat) have not been published. The most comprehensive published FOWT scale test was performed in the United States by collaboration between the National Renewable Energy Laboratory, NREL, and the University of Maine, UMaine. Experiences from this test are reviewed in the following. Further, a review of relevant scaling laws and a list of relevant publications addressing this issue are provided.

3.1.1 List of Symbols for the review

| | |
|----------|--|
| c_s | = speed of sound |
| C | = wave celerity |
| Fr | = Froude number |
| g | = acceleration of gravity |
| l | = characteristic length |
| KC | = Keulegan-Carpenter number |
| Ma | = Mach number |
| Ω | = rotor angular velocity [radians/sec] |
| ρ | = fluid density |
| R | = blade radius |
| Re | = Reynolds number |
| St | = Strouhal number |
| TSR | = tip speed ratio |
| μ | = fluid dynamic viscosity |
| U | = free stream fluid velocity |

3.1.2 Important Non-Dimensional Numbers

Non-dimensional numbers are dimensionless fractions or products resulting from relations between parameters defined by the fundamental quantities L, M, and T (length, mass, and time, respectively). The two most important non-dimensional numbers to conserve when modeling a scaled rotor system are the Lock Number and the Reynolds Number [27,28]. These reflect the most important parameters involved with aerodynamic and elastic forces. The Froude Number is the most important non dimensional number to preserve when modeling floating structures for hydrodynamic similarity [29,30].

Geometric Scaling Factor (λ)

The geometric scaling factor describes the ratio of the physical length between the full scale turbine and the scaled test model. The value of λ is constrained by the size of the testing facility, feasibility of model construction, scaling law similitude requirements, and the project's budget.

Froude Number (Fr)

The Froude number is a dimensionless number that defines the ratio of inertial forces to gravitational forces in a fluid. When a free surface wave propagates within a fluid, the Froude number can be defined in the following way [29]:

$$(3.1.1) \quad Fr_{\text{wave}} = C / (gl)$$

In wind-wave basin model tests, the Froude number is the most frequently conserved dimensionless number to ensure hydrodynamic similitude. While viscous effects do affect FOWT platform hydrodynamics, they are considered small in comparison to inertial effects at both test and model scales. Viscous effects are mostly manifested in the thin boundary layer around floating bodies [31].

Reynolds Number (Re)

The Reynolds number is defined as the ratio of inertial forces to viscous forces in a flow. For a cylinder exposed to a fluid with velocity u , the Reynolds number is

$$(3.1.2) \quad Re = \rho DU / \mu$$

The Reynolds number is important in fluid systems because qualitatively, flow over a body acts similarly for identical Reynolds numbers. Hereby e.g. lift and drag coefficients can be parameterized in terms of the Reynolds number [33]. Because of the small length scales at which models are tested, there is almost always Reynolds number mismatch between model and full scales that cannot be resolved unless there is a change in the fluid of the system (i.e. viscosity or density) [27,32]. Although this has been done successfully in the helicopter industry, we believe it is out of the scope of existing wind-wave basin test facilities. This mismatch is often combated by using airfoils that have coefficients of lift and drag with minimal dependence on Reynolds number. This is especially important in the low Reynolds number regimes encountered in model testing [27].

Keuligan-Carpenter number (KC)

The Keuligan-Carpenter number is a characteristic number for planar oscillatory flows defined as

$$(3.1.3) \quad KC = U_m T_w / D,$$

where U_m is the maximum velocity in the outer flow, T_w is the period of the flow and D is the cylinder diameter. It provides a measure for the length of a horizontal particle path in the outer flow relative to the cylinder diameter. For

small KC numbers, there will be no flow separation around the cylinder, where for large KC numbers, vortex shedding will occur during the flow cycle. As a rule of thumb, the balance between inertia and viscous forces is equal to $20/KC$ [15]. Small KC numbers thus implies dominant inertial loading, while large KC numbers are associated with dominant viscous loading.

Tip Speed Ratio (TSR)

The tip speed ratio is the ratio of the rotor's velocity to the wind's free stream velocity:

$$(3.1.4) \quad \text{TSR} = \Omega R / U$$

Maintaining a constant TSR is one of the most basic procedures used to preserve similarity in scaling a wind turbine system [34]. If the TSR and the geometry of the blades are scaled similarly, the flow geometry over the blades will be preserved. This statement is only an approximation because the Reynolds number will vary as the scale of the blade changes, therefore causing flow dissimilarity. However, TSR consistency should still be realized in model testing, and is compatible with Froude similitude when used to constrain rotational frequencies and wind speed [29].

Mach Number (Ma)

The Mach number is the ratio of the flow velocity to the speed of sound, and is an influential parameter in gas dynamics [35]:

$$(3.1.5) \quad \text{Ma} = U / c_s$$

The conservation of the Mach number is often employed in aerodynamic model scaling because it characterizes compressibility effects [30]. At Mach numbers below 0.3, flow can be considered incompressible [35]. Figure 3.1.1 depicts the Mach number for a full size and model size (1:45) NREL 5 MW reference rotor. It is seen that compressibility effects can be ignored at both scales because the Mach number remains below 0.3. This means that conserving the Mach number's exact value between scales is not necessary for aerodynamic similitude [29].

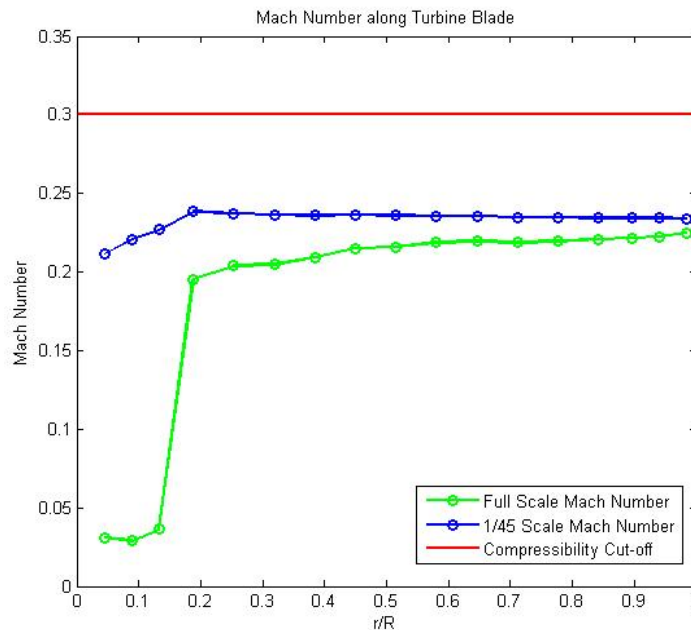


Figure 3.1.1. Mach number calculation for a full scale NREL 5 MW reference turbine and its 1/45th scale model (calculated using BEM theory) [29]. The Mach numbers in both systems are below 0.3, which validates the assumption of incompressible flow at full and model scales. This data was generated in a simulation where the wind speed was 11.4 m/s and the rotor TSR was 6.958.

Strouhal Number (St)

The Strouhal number is the dimensionless vortex shedding frequency for a body emerged in a viscous fluid

$$(3.1.6) \quad St = f D / V$$

If Froude scaling is employed, the Strouhal number cannot always be maintained because of its dependence on the Reynolds number. However, the Strouhal number stays at a value of 0.2 for a range of Reynolds number and its effects have been neglected in past experiments [29]. The Strouhal number is typically conserved to ensure similitude in vortex induced vibration (VIV) driven effects, which may not be important for FOWT (specifically TLP) model testing.

3.1.3 Dominant scaling methodologies for FOWT

Geometric Scaling

The simplest method of creating a scale model is to scale the full turbine's geometry by a factor of λ , thereby creating a miniature turbine that preserves all relative length dimensions. However, the performance of turbines at different length scales depends on more than their geometry and crucial dissimilarities will exist if this is the only scaling method chosen. For instance, every non-dimensional number (except λ) in the previous section depends on environmental parameters independent of the model's geometry, meaning that the dynamic and kinematic effects described by such non-dimensional numbers will differ between the model and full scale turbines unless efforts are made to equate the values of these numbers at all scales.

Dynamic and Elastic Scaling

In order for model size turbines to act dynamically similar to full size turbines, one must ensure that the model's aerodynamics and hydrodynamics match those of the full scale system [31]. Additionally, dynamic similarity requires that natural frequencies and gyroscopic moments are properly scaled from the full to model scale [36]. It has been well established by the oil and gas industry that Froude number equality between the model scale and full scale is most effective in achieving hydrodynamic similarity. Froude scaling has been successfully applied in several model studies of floating wind turbines including those of NREL and UMAINE.

Froude scaling has further been validated by NREL FAST simulations [36]. However, these tests assume that Reynolds number dependent aerodynamic parameters (airfoil C_l , C_d , and viscous damping) were kept constant between model and full scales, an assumption that is difficult to realize in physical modeling. In addition to Froude scaling, the TSR should be held constant at different scales in order to yield consistency in FOWT kinematics and flow geometries. This will be further detailed in this report.

The scaling methodology proposed in this report is the dynamic and elastic scaling, based on preservation of the Froude number and tip speed ratio. This will be detailed in section 3.2.

3.1.4 UMAINE scaled FOWT testing review

The University of Maine designed their tower to mimic the dynamic behavior of the OC3 Hywind tower by scaling the lowest frequency modes and center of gravity according to Froude similarity [29]. The mass of the tower failed to directly follow Froude scaling, because a mass-scaled tower construction was impractical and difficult in initial



designs. UMaine justified and compensated for this dissimilarity by scaling the combined mass of the tower, nacelle, and rotor. The nacelle was overweight, and the lightweight tower would help compensate. The tower had a fore-aft fundamental bending frequency that was only 5.4% lower than desired and the center of gravity for the model was 3.3% higher than desired [29]. The model tower diameter was 3.7 times smaller than a Froude scaled diameter, and UMaine considered this to be advantageous because it decreased aerodynamic interaction between the tower and the turbine, something the available NREL software could not simulate [37,29].

University of Maine's goal when designing blades was to keep them lightweight and to have the airfoil cross sections to remain as consistent as possible with the full scale model. Priority was given to gathering information about the global responses of the FOWT system, not the "blade deformation, rotor dynamics, and higher order aero-elastic effects" [29].

Geometric redesign was also avoided. Blades were constructed out of carbon fiber to eliminate as much blade flexibility as possible and reduce the number of variables in testing. This made blade tip deflections negligible and limited the chances of blade failure during experiments. The low weight of carbon fiber was advantageous because of the small blade mass required for Froude consistency in rotor mass and gyroscopic moments.

A mold and bladder process was used to fabricate 15 blades with a mass of 0.130 kg. This was .010 kg lower than Froude scaled mass, which benefited UMaine by making up for the overweight nacelle and testing wires [29].

The blade deflections were only 2% of theoretical maximum blade deflections, which satisfied UMaine because of the blade's near-rigid nature. The rotor was unable to produce Froude scaled thrust when the testing wind speed was constrained by the wind speed to wave celerity ratio (α), so tests were run in faster winds. Doing so eliminated the possibility of testing at *TSR*'s higher than five, because the rotor had not been designed for such high angular velocities [36].

Besides the scaling issues described above, UMAINE used a cable to collect the data from the FOWT, that might have influenced the floater motions during the test. Therefore it is recommended, that a lightweight cable or a wireless data acquisition system is used in future tests.

3.2 RECOMMENDED SCALING METHOD

The proposed scaling method is derived in this section. It is consistent with the one described by Martin [29] apart from the inclusion of a different water density at prototype scale and model scale in the present scaling. Such a difference will often occur due to the use of fresh water in model tests, opposed to the sea water at prototype scale.

For model tests with combined wind and wave forcing, the main interest is the global motion of the structure subject to the aero- and hydro-dynamic loads plus the loads from mooring and gravity. The ratio of these loads must therefore be preserved between prototype scale and model scale. Further, as the loads are dynamic in time, the frequencies of the loads, the structural frequencies and the rotor frequency must scale consistently. These requirements define the scaling of all relevant quantities and are derived in the following. The scaling can be applied to e.g. model tests of floating wind turbines, as illustrated in Figure 3.2.1. The proposed scaling preserves the Froude number and KC number for the hydrodynamic motion and the tip speed ratio for the rotor. The Reynolds number for water and air, however, are not preserved. This leads to the requirement of a re-design of the blades to achieve the correct thrust force. Further, the invariance of the hydrodynamic force coefficients (inertia and drag coefficients) to the hydrodynamic Reynolds number should be checked and significant differences be compensated, see e.g. [44]. Also, but of less practical impact, the Weber number for water (surface tension) and Mach number for air (compressibility) are not preserved.

It should also be noted that while the proposed scaling leads to a consistent thrust force from the rotor, the re-designed blades at the model scale Reynolds number might not reproduce a consistent rotor torque. This will lead to an inconsistent power production and an inconsistent dynamic generator moment. The latter moment contributes to the roll-forcing of the platform. Hence, to avoid this imperfection, a reproduction of the aerodynamic torque of the re-designed blades should be pursued. Most important, as already mentioned, however, is a correct thrust-reproduction.

3.2.1 Scaling of geometric length and mass properties

The geometric length scale ratio is defined by

$$(3.2.1) \quad \lambda = \frac{L_p}{L_m}$$

For a correct dynamic scaling the ratio of structural mass and displaced water mass must be preserved:

$$(3.2.2) \quad \frac{M_p}{\rho_{wp} \text{vol}_p} = \frac{M_m}{\rho_{wm} \text{vol}_m}$$

As the volume scales like λ^3 this yields

$$(3.2.3) \quad \frac{M_p}{M_m} = \frac{\rho_{wp}}{\rho_{wm}} \lambda^3$$

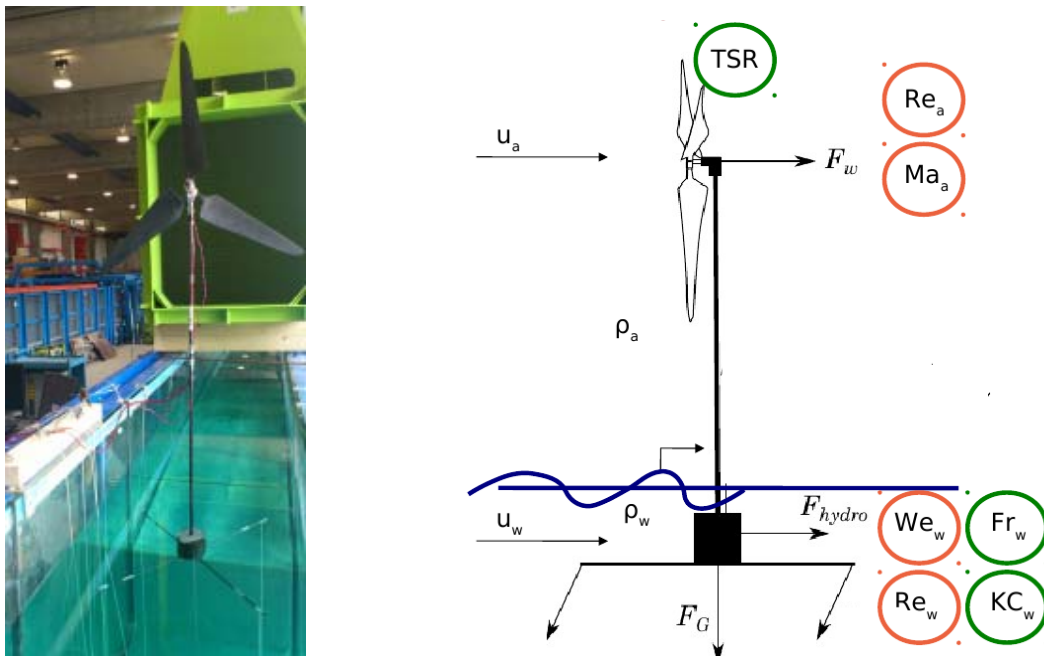


Figure 3.2.1: A floating wind turbine in a wave flume with open jet wind tunnel at DTU (Hansen & Laugesen [38]). The sketch to the right shows the forces involved. The circled quantities are dimensionless numbers that characterise the environment and the motion.

This defines the scaling of the mass moment of inertia J

$$(3.2.4) \quad \frac{J_p}{J_m} = \frac{\int_{M_p} r_p^2 dM_p}{\int_{M_m} r_m^2 dM_m} = \frac{\rho_{wp}}{\rho_{wm}} \lambda^5$$

and the scaling of the area moment of inertia for a structural cross section I

$$(3.2.5) \quad \frac{I_p}{I_m} = \frac{\int_{A_p} r_p^2 dA_p}{\int_{A_m} r_m^2 dA_m} = \lambda^4$$

3.2.2 Froude scaling of hydrodynamic forces

A correct dynamic scaling requires that the ratio of inertial force to gravitational force is preserved

$$(3.2.6) \quad \frac{\rho_{wp} A_p u_{wp}^2}{\rho_{wp} \text{vol}_p} = \frac{\rho_{wm} A_m u_{wm}^2}{\rho_{wm} \text{vol}_m} \Rightarrow \frac{u_{wp}}{u_{wm}} = \lambda^{1/2}$$

Further, the travelled distance of a water particle over a given time must scale with the geometric length:

$$(3.2.7) \quad \frac{u_{wp} t_p}{L_p} = \frac{u_{wm} t_m}{L_m} \Rightarrow \frac{t_p}{t_m} = \lambda^{1/2}$$

which defines the global time scale. This constitutes the classical Froude scaling of the hydrodynamic forces and motion.

3.2.3 Aerodynamic scaling

For dynamic similarity, the ratio of the aerodynamic thrust force to the gravity force on the structure must be preserved

$$(3.2.8) \quad \frac{\frac{1}{2} \rho_{ap} C_{Tp} A_p u_{ap}^2}{M_p g} = \frac{\frac{1}{2} \rho_{am} C_{Tm} A_m u_{am}^2}{M_m g} \Rightarrow \frac{u_{ap}}{u_{am}} = \sqrt{\frac{C_{Tm}}{C_{Tp}} \frac{\rho_{wp}}{\rho_{wm}} \lambda}$$

It is desirable that the relative velocity between the structure and air is preserved. Therefore the air velocities must scale like $\lambda^{1/2}$. It is therefore necessary to scale the C_T values with the density ratio to obtain.

$$(3.2.8) \quad \frac{C_{Tp}}{C_{Tm}} = \frac{\rho_{wp}}{\rho_{wm}} \quad \frac{u_{ap}}{u_{am}} = \lambda^{1/2}$$

Hereby, however, the proposed scaling will not preserve the Reynolds number in the air or water. For this reason a re-design of the blades will be needed to obtain the desired value of C_{Tm} .

The chosen scaling, however, preserves the tip speed ratio (TSR)

$$(3.2.9) \quad \text{TSR}_p = \frac{\Omega_p R_p}{u_{ap}} = \frac{\Omega_m R_m}{u_{am}} = \text{TSR}_m$$

as the rotor frequency scales inversely with time $\Omega_p / \Omega_m = \lambda^{-1/2}$.

3.2.4 Scaling of structural stiffness

The structural stiffness must be scaled such that the natural frequencies scale consistently with time. Further the structural deflection must scale directly with the length scale. The appropriate scaling can be derived from the dynamic beam equation

$$(3.2.10) \quad \rho_s A \frac{\partial^2 x}{\partial t^2} + \frac{\partial^2}{\partial z^2} \left(EI \frac{\partial^2 x}{\partial z^2} \right) = p$$

Here $\rho_s A$ is the structural mass per length, x transverse deflection, z the spatial coordinate along the beam axis, E Young's modulus, I area moment of inertia and p the transverse load per unit length. It is observed that the first term on the left hand side and the transverse load term scale like $(\rho_{wp}/\rho_{wm})\lambda^2$ while the middle term scales like $E\lambda$. A consistent scaling of the equation of motion is therefore obtained for

$$(3.2.11) \quad \frac{E_p}{E_m} = \frac{\rho_{wp}}{\rho_{wm}} \lambda$$

3.2.5 Check of natural frequency and gyroscopic force

The above derivation defines the necessary scaling. A check on the natural frequency and gyroscopic force is provided. The natural frequency of a cantilever beam of length L is given by

$$(3.2.12) \quad f_N = \frac{1}{2\pi} 1.875^2 \sqrt{\frac{EI}{\rho_s AL^4}}$$

Application of the above scaling yields

$$(3.2.12) \quad f_N = \frac{1}{2\pi} 1.875^2 \sqrt{\frac{EI}{\rho_s AL^4}} \sim \sqrt{\frac{\frac{\rho_{wp}}{\rho_{wm}} \lambda \lambda^4}{\frac{\rho_{wp}}{\rho_{wm}} \lambda^2 \lambda^4}} = \lambda^{-1/2}$$

which is consistent with the time scaling $t \sim \lambda^{1/2}$.

The gyroscopic moment from the change of the orientation of the rotor is

$$\tau = \frac{d}{dt} (\omega J)$$

where ω is the rotational vector and J is the mass moment of inertia. The gyroscopic moments scales according to

$$(3.2.13) \quad \tau = \frac{d}{dt} (\omega J) \sim \frac{1}{\lambda^{1/2}} \left(\lambda^{-1/2} \frac{\rho_{wp}}{\rho_{wm}} \lambda^5 \right) = \frac{\rho_{wp}}{\rho_{wm}} \lambda^4$$

which is consistent with the scaling of force times length.

3.2.6 Properties that may not scale consistently

It has already been mentioned that certain properties will not scale consistently with the proposed scaling. These are

1. the aero- and hydro-dynamic Reynolds numbers.
2. the hydrodynamic Weber number
3. the aerodynamic Strouhal number
4. the aerodynamic Mach number
5. the aerodynamic torque
6. the aerodynamic power
7. the generator torque and its contribution to roll-forcing

While (1) is compensated by a re-design of the blades and a check of the hydrodynamic drag and inertia coefficients, (2-6) are considered of small significance for the global planar motion of the wind turbine. The scaling thus ensures a consistent in-plane motion of the floating wind turbine. For the out-of-plane motion (sway, roll, yaw) the gyroscopic moments will scale correctly, while the roll-forcing from a dynamic generator torque (7) will not necessarily scale correctly. A correction of this effect is open for future research.

3.2.7 Summary of the scaling

The proposed scaling is summarised in Table 3.2.1

| Property | Scaling factor |
|------------------------------|---------------------------------------|
| Length | λ |
| Mass | $(\rho_{wp}/\rho_{wm}) \lambda^3$ |
| mass moment of inertia (J) | $(\rho_{wp}/\rho_{wm}) \lambda^5$ |
| area moment of inertia (I) | λ^4 |
| Velocity | $\lambda^{1/2}$ |
| acceleration | 1 |
| Time | $\lambda^{1/2}$ |
| frequency | $\lambda^{-1/2}$ |
| Angle | 1 |
| Force | $(\rho_{wp}/\rho_{wm}) \lambda^3$ |
| Moment | $(\rho_{wp}/\rho_{wm}) \lambda^4$ |
| stiffness (E) | $(\rho_{wp}/\rho_{wm}) \lambda$ |
| Stress | $(\rho_{wp}/\rho_{wm}) \lambda$ |
| Power | $(\rho_{wp}/\rho_{wm}) \lambda^{7/2}$ |
| Thrust coefficient (C_T) | (ρ_{wp}/ρ_{wm}) |

Table 3.2.1 Summary of physical quantities and scaling factors.

3.3 SCALING OF WIND AND WAVE CLIMATE PARAMETERS

The dynamic and elastic scaling can be directly applied to the wind and wave climates to scale from prototype scale to model scale, as the scalings for length and velocity has been defined. This yields the following scaling:

| Property | Scaling factor |
|---|------------------|
| geometric height (z) | λ |
| wind speed (V) | $\lambda^{1/2}$ |
| turbulent wind spectrum S_w | $\lambda^{3/2}$ |
| turbulent wind frequency (f) | $\lambda^{-1/2}$ |
| turbulence intensity | 1 |
| wind profile power coefficient (α) | 1 |
| water depth | λ |
| velocity | $\lambda^{1/2}$ |
| significant wave height | λ |
| peak period | $\lambda^{1/2}$ |
| wind-wave misalignment | 1 |

Table 3.3.1. Scale relations for wind and wave climate.

3.4 EXAMPLE: SCALED EXPERIMENT OF A FLOATING WIND TURBINE

In the following the scaling procedure is illustrated with a numerical example. A simple model for a TLP floating wind turbine is derived. The wind turbine is subjected to stochastic wind and wave loads at prototype scale. Next, the wind climate, wave climate and wind turbine are scaled to scale 1:50 and the small-scale response is computed in the numerical model. The prototype-scale and small scale responses moment are compared. It is demonstrated that a perfect scaling can be achieved if the aerodynamic thrust and hydrodynamic loads are reproduced correctly at model scale. Imperfections due to incomplete aerodynamic scaling are discussed.

3.4.1 The TLP wind turbine

The wind turbine is the NREL 5 MW reference turbine (Jonkman et al [39]) placed on the NREL-MIT TLP platform (Matha [40]). A sketch of the structure is shown in Figure 3.4.1. The purpose of the example is to illustrate the scaling in a simplified setting that includes hydrodynamic forces from a wave climate, aerodynamic forces from a wind climate, gravitational forces and structural elasticity. Only two degrees of freedom are retained and several simplifying assumptions are made. These are listed below

- only two degrees of freedom are considered: platform surge and tower flexibility
- the tower is considered mass-less and with uniform stiffness. The original tower mass is distributed onto the top mass and the floater mass.
- small deflections for the platform is assumed
- the tethers are assumed mass-less and stiff
- the rotor mass, nacelle mass are considered as a point mass, placed on top of the tower. Half of the original tower mass is included.
- the floater is considered slender ($D/L < 0.2$)
- the waves are considered small to allow application of linear wave theory
- spatially coherent turbulence is assumed

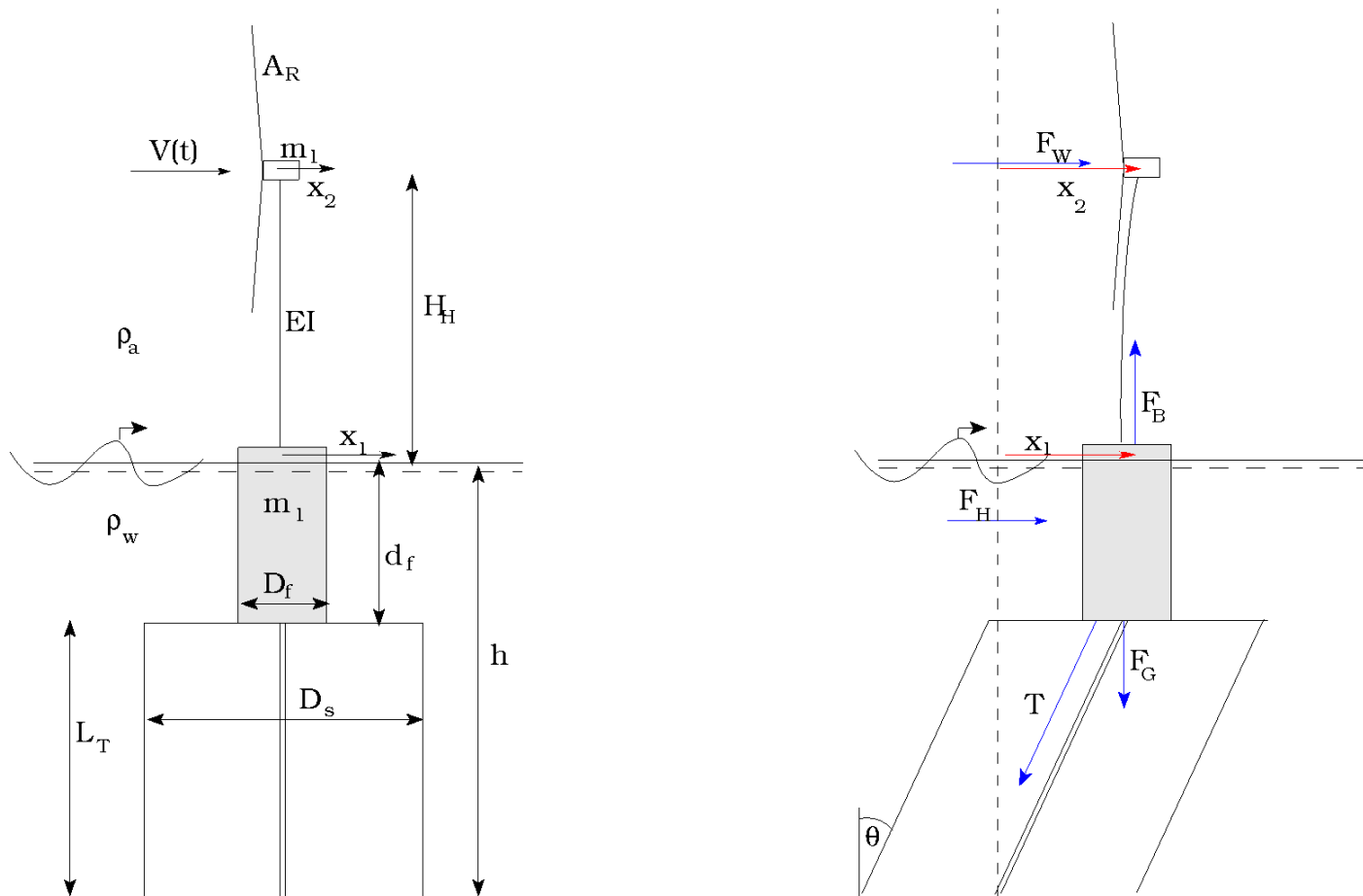


Figure 3.4.1. Model sketch for simple model of a TLP wind turbine.

The structural parameters are listed in Table 3.4.1.

| Property | Symbol | Value prototype scale | Scaling | Value, model scale (1:50) |
|------------------|----------|--------------------------|-----------------------------------|---------------------------|
| Floater mass | m_1 | 8.774×10^6 kg | $(\rho_{wp}/\rho_{wm}) \lambda^3$ | 68.48 kg |
| Top mass | m_2 | 518.5×10^3 kg | $(\rho_{wp}/\rho_{wm}) \lambda^3$ | 4.047 kg |
| Tower stiffness | EI | 300×10^9 Pa | $(\rho_{wp}/\rho_{wm}) \lambda^5$ | 936.6 Pa |
| Hub height | H_H | 90m | λ | 1.80 m |
| Floater diameter | D_f | 18m | λ | 0.36 m |
| Floater draft | d_f | 47.89m | λ | 0.958 m |
| Water depth | h | 200m | λ | 4.00 m |
| Tether length | L_T | 152.11m | λ | 3.04 m |
| Rotor diameter | D_R | 126m | λ^2 | 2.52 m |
| Density of air | ρ_a | 1.29 kg/m ³ | 1 | 1.29 kg/m ³ |
| Density of water | ρ_w | 1025 kg/m ³ | ρ_{wp}/ρ_{wm} | 1000 kg/m ³ |

Table 3.4.1: Parameters for floating wind turbine at full scale and model scale.

3.4.2 Equations of motion

The equations of motion consist of Newton's second law for the floater and the top mass. The displacement of the masses relatively to an earth-fixed reference point is denoted x_1 and x_2 , respectively, as shown in Figure 3.4.1. The restoring force from the mooring system can be derived by calculation of the excess buoyancy force F_{BE}

$$(3.4.1) \quad F_{BE} = \rho_w g \frac{\pi}{4} D_f^2 d_f - (m_1 + m_2)g$$

which constitutes the vertical component of the total tether force T . Next, the force triangle for the tether force, excess buoyancy force and horizontal tether force F_x gives

$$(3.4.2) \quad F_x / F_{BE} = \tan \theta$$

where θ is the tether angle with vertical, measured positive in the counter-clockwise direction. Under the assumption of small deflection angles, this is approximated by $-x_1/L_T$ whereby

$$(3.4.3) \quad F_x = -\frac{F_{BE}}{L_T} x_1$$

The elastic bending of the tower constitutes the connection force between the tower and floater, tower and top mass, respectively. The tower is considered mass-less and no dynamic loads are thus associated with the tower. From standard Euler-Bernoulli beam theory, the force needed to displace the end point of a cantilever beam by a distance x is $F=3 EI x/L^3$, where EI is the stiffness and L is the length. The equations of motion can thereby be expressed as

$$(3.4.4a) \quad (m_1 + A_{11})\ddot{x}_1 + \frac{F_{BE}}{L_T} x_1 = \frac{3EI}{H_H^3} (x_2 - x_1) + F_H$$

$$(3.4.4b) \quad m_2 \ddot{x}_2 = \frac{3EI}{H_H^3} (x_1 - x_2) + F_W$$

where F_H is the hydrodynamic excitation force, A_{11} is the hydrodynamic added mass for the floater (derived in next paragraph) and F_W is the aerodynamic thrust force from the wind.

3.4.3 Hydrodynamic force

The hydrodynamic loading is derived from simple linear wave theory under the assumption of small wave steepness. The free surface elevation η is expressed as a Fourier series

$$(3.4.5) \quad \eta = \sum_{p=1}^N a_p \cos(\omega_p t - k_p x + \xi_p)$$

where the amplitudes a_p are related to the wave spectrum by

$$(3.4.6) \quad a_p = \sqrt{2S_\eta(f) \Delta f}$$

and the radian frequency ω_p and wave number k_p are related through the dispersion relation

$$(3.4.7) \quad \omega^2 = gk \tanh kh$$

and further ξ_p is a set of random phases, uniformly distributed on the interval $[0;2]\pi$.

The horizontal fluid velocities are given by

$$(3.4.8) \quad u = \sum_{p=1}^N a_p \frac{gk_p}{\omega_p} \frac{\cosh(k_p(z+h))}{\cosh(kh)} \cos(\omega_p t - k_p x + \xi_p)$$

and allows computation of the hydrodynamic force on a horizontal cross-section of height dz through the Morison equation [45] under the assumption of small floater diameter to wave length:

$$(3.4.9) \quad dF = \rho_w C_m A_f (u_t - \ddot{x}_1) dz + \rho_w A_f u_t dz + \frac{1}{2} \rho_w C_D D_f (u - \dot{x}_1) |u - \dot{x}_1| dz$$

Here C_m is the hydrodynamic added mass coefficient, C_D is the drag coefficient and A_f is the cross-sectional area of the floater. Still under the approximation of linear wave theory, the hydrodynamic forcing is integrated from the bottom of the floater to the still water level. Further, the contribution from $x_{1,tt}$ is moved to the left hand side where it forms the A_{11} term of the mass matrix:

$$(3.4.10) \quad F_H = \int_{z=-d_f}^0 \rho_w (C_m + 1) A_f u_t dz + \int_{z=-d_f}^0 \frac{1}{2} \rho_w C_D D_f (u - \dot{x}_1) |u - \dot{x}_1| dz$$

$$(3.4.11) \quad A_{11} = \rho_w C_m A_f d_f$$

The hydrodynamic coefficients are chosen based on the Reynolds number and KC number to be $C_D=0.7$ and $C_m=0.8$.

3.4.4 Aerodynamic force

The wind force is based on a time series of horizontal wind velocity at hub height

$$(3.4.12) \quad V(t) = V_{\text{hub}} + \sum_{m=1}^M b_m \cos(\omega_m t + \epsilon_m)$$

where V_{hub} is the mean wind speed at the hub and the Fourier amplitudes are based on the wind spectrum S_f

$$(3.4.13) \quad b_p = \sqrt{2S_f(f) \Delta f}$$

and further ϵ_m is a set of random phases, uniformly distributed on the interval $[0;2]\pi$. The instantaneous thrust can then be expressed by:

$$(3.4.14) \quad F_{\text{wind}} = \frac{1}{2} \rho_a A_{\text{Rotor}} C_T (V - \dot{x}_2) |V - \dot{x}_2|$$

where C_T is the thrust coefficient. Under the approximation of steady wind speed, C_T can be obtained from a steady BEM model as function of wind speed, see e.g. Hansen [41]. The curve applied in the present example is shown in



Figure 3.4.2 and resembles the one for the NREL 5MW reference rotor. In the same figure, also the thrust force F_{wind} is plotted. It is seen how the thrust force increases up to the rated speed of 11.4 m/s, where the rated power of 5MW is obtained. Beyond the rated wind speed, the thrust force decreases due to the active blade pitch system, which pitches the blades to reduce the aerodynamic torque in order to maintain the rated power.

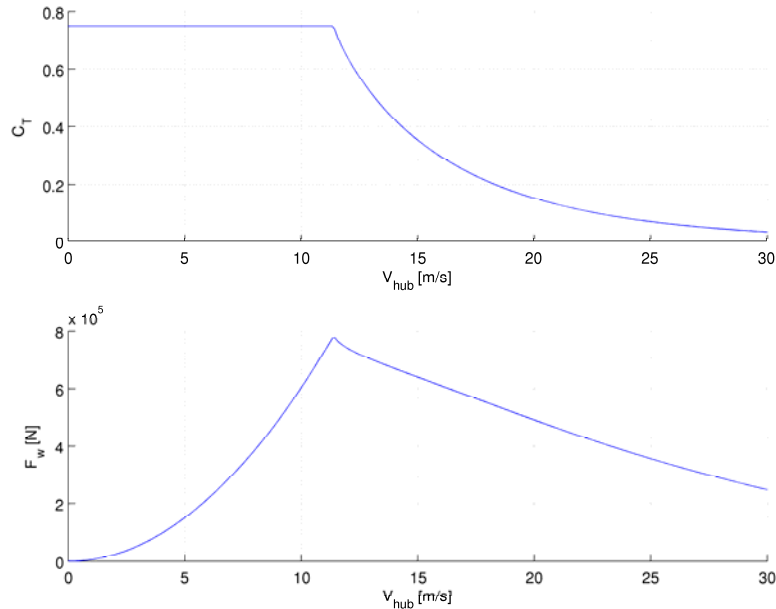


Figure 3.4.2. Thrust coefficient and thrust as function of inflow speed V .

The pitching of the blades is controlled by an active control system. It has been shown by Larsen and Hanson [42] that the standard on-shore control algorithm can lead to an instability for the platform pitch motion. The control system therefore needs to be modified. In the present simplistic model, a simple P-control is used to model the reaction time of the blade-pitching, based on the instantaneous difference between the current C_T value and the target C_T value for the instantaneous relative wind speed $V-x_{2,t}$.

3.4.5 Wind and wave climate

Based on the generic wave and wind climates of section 2.4, a set of prototype wind and wave conditions are now chosen. Next, the climate parameters are scaled to model scale.

The Weibull distributions for wind height at $z=10m$ of Figure 2.4.1 can be transformed to the hub height by a scaling of the A parameter by the assumed power-law profile. It is further assumed that the shape parameter, k , does not change with height. The approximation associated with this is discussed in section 2.

$$(3.4.15) \quad \frac{V_{hub}}{V_{10}} = \left(\frac{90 \text{ m}}{10 \text{ m}} \right)^{0.14} = 1.36 \quad \Rightarrow \quad A_{Weibull \text{ hub}} = A_{Weibull 10} \times 1.36$$

The adjusted Weibull parameters provide a complete probability distribution for the mean wind speed at hub height. For the present example, we choose a single climate for a single realization with the numerical model. We choose a hub wind speed of $V_{hub}=18m/s$. Next, the turbulence intensity is found by the formula (2.3.5) which with $a=5$ and $l_{15}=0.14$ yields

$$(3.4.16) \quad TI = \frac{15 + aV}{(1 + a)V} I_{15} = 0.136$$

The standard deviation to be used in combination with the Kaimal spectrum is then $\sigma = TI V = 2.45$ m/s. Next the significant wave height is chosen with basis in Figure 2.4.3. We choose the fitted curve for the relation between V_{hub} and H_s (2.4.1) and obtain

$$(3.4.18) \quad \frac{H_s}{H_{s0}} = 1 + 2.6 \frac{(V/V_0)^3}{1 + (V/V_0)^2} = 3.37 \quad \Rightarrow \quad H_s = 3.37 \text{ m}$$

The peak period is chosen based on Figure 2.4.4 which shows quite some scatter. Rather arbitrarily a value of $a=12$ for the coefficient in formula (2.4.2) is chosen to yield

$$(3.4.19) \quad T_p = 12 \sqrt{H_s/g} = 7.03 \text{ s}$$

Finally, for the Jonswap spectrum, γ needs to be determined. Here formula (2.3.11) suggests $\gamma = 3.83$ which seems unrealistic as it exceeds the standardized value of 3.3. For this reason $\gamma = 3.3$ is chosen. It should be noted here that for a floating wind turbine, the depth will usually be large such that the Pierson Moscovitz spectrum is likely to be more realistic. This is recovered with reason $\gamma = 1.0$. However, for the present example $\gamma = 3.3$ is applied.

Once the wind- and wave climate parameters are determined, they can be scaled to model scale according to Table 3.4.1. The result is listed in Table 3.4.2 along with the prototype values and the scale relation.

| Property | Symbol | Value prototype scale | Scaling | Value, model scale (1:50) |
|------------------------------------|-----------|-----------------------|-----------------|---------------------------|
| hub height | z_{hub} | 90 m | λ | 1.8 m |
| wind speed 10m height | V_{10} | 13.2 m/s | $\lambda^{1/2}$ | 1.87 m/s |
| hub wind speed | V | 18 m/s | $\lambda^{1/2}$ | 2.55 m/s |
| power law coefficient | α | 0.14 | 1 | 0.14 |
| turbulence intensity | TI | 0.136 | 1 | 0.136 |
| standard deviation for turbulence | σ | 2.45 m/s | $\lambda^{1/2}$ | 0.347 m/s |
| length scale for Kaimal spectrum | L | 340.2m | λ | 6.80 m |
| Wind velocity Fourier amplitude | b | From eq (3.4.13) | $\lambda^{1/2}$ | From eq (3.4.13) |
| significant wave height | H_s | 3.37 m | λ | 0.0674 m |
| peak period | T_p | 7.03 s | $\lambda^{1/2}$ | 0.994 s |
| Jonswap peak enhancement parameter | γ | 3.3 | 1 | 3.3 |

Table 3.4.2. Wind and wave climate. Prototype scale and model scale.

3.4.6 Results for perfect aerodynamic scaling

Results for the realization at prototype scale are shown in Figure 3.4.3. The left column shows time series of wind speed at hub height, free surface elevation for the waves, floater displacement and nacelle displacement. The right column shows the corresponding power spectra. It can be seen that the wind signal has spectral energy in the full frequency interval shown, while the wave signal does not have any energy for frequencies below 0.1 Hz. Further, the floater surge signal is dominated by the response to the wind at the first natural frequency of 0.017 Hz (60 s) which is associated with the restoring force of the tethers. Response to the wave forcing is evident both from the time series and the power spectrum. For the nacelle displacement, a similar response can be seen, although with a larger content of tower-vibration. This is due to the winds forcing of the tower natural frequency at 0.25 Hz (4s).

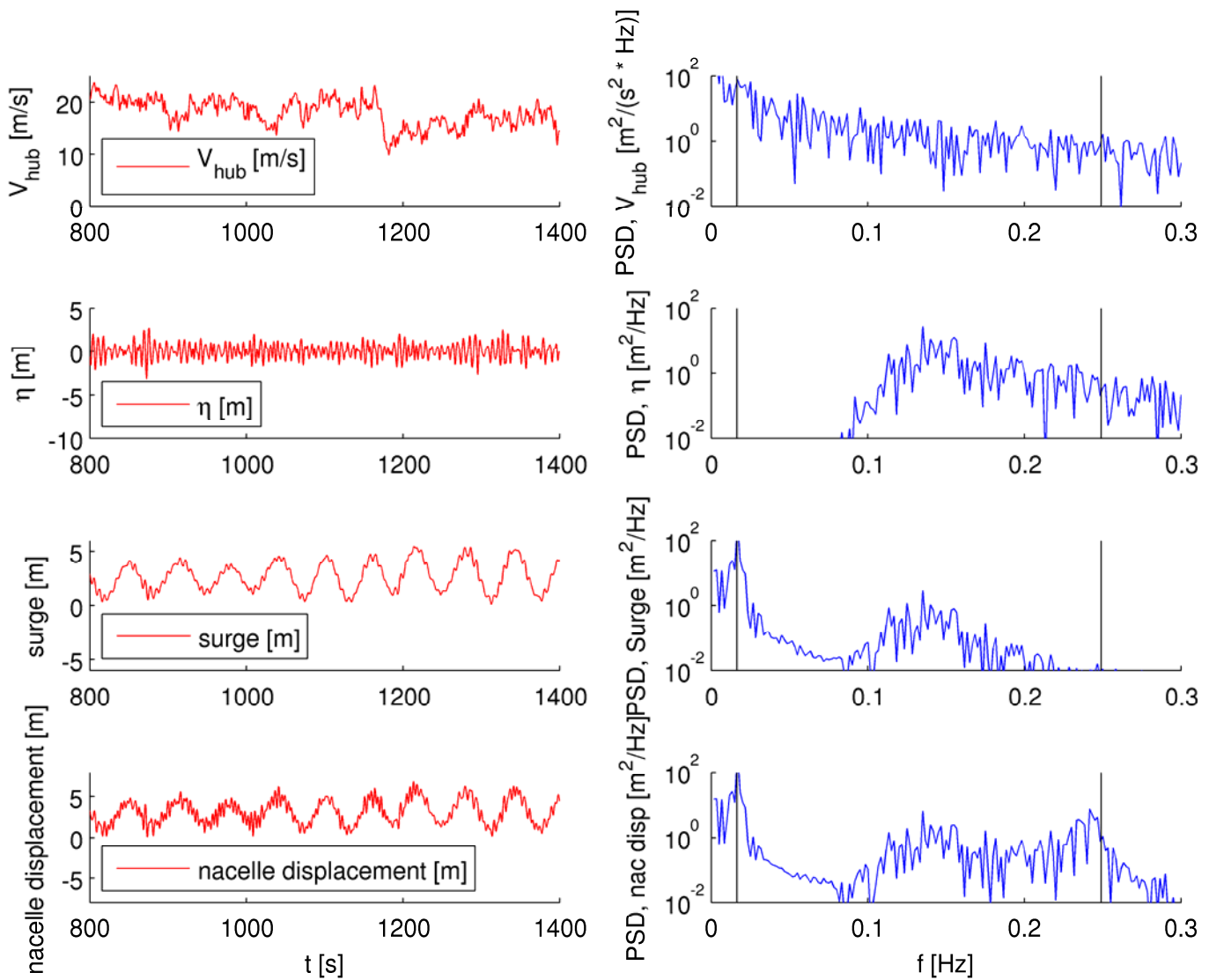


Figure 3.4.3. Response at prototype scale for simultaneous wind and wave loading.

Next, the numerical model was re-run at model scale. All the model parameters and external climate parameters were scaled according to Tables 3.2.1 and 3.3.1. The scaled parameter values are listed in Tables 3.4.1 and 3.4.2. The numerical time series are shown in Figure 3.4.4, plotted on top of the full-scale values. Prior to the comparison, the

model-scale results were scaled up again to prototype scale. The model scale results are shown as black dots on top of the prototype scale results (red line). A perfect match is seen. In hindsight, this is not a surprise, since the scaling is consistent with the governing equations. The example thus illustrates that it is possible to scale down the wind and wave climates and scale back the model response to full scale. The good match, however, relies on the models ability to reproduce the aerodynamic (and hydrodynamic) loads at model scale. For both of them, the Reynolds number dependence is likely to induce scale effects. As already stated, a re-design of the blades will be thus necessary to maintain the thrust-curve at the reduced Reynolds number.

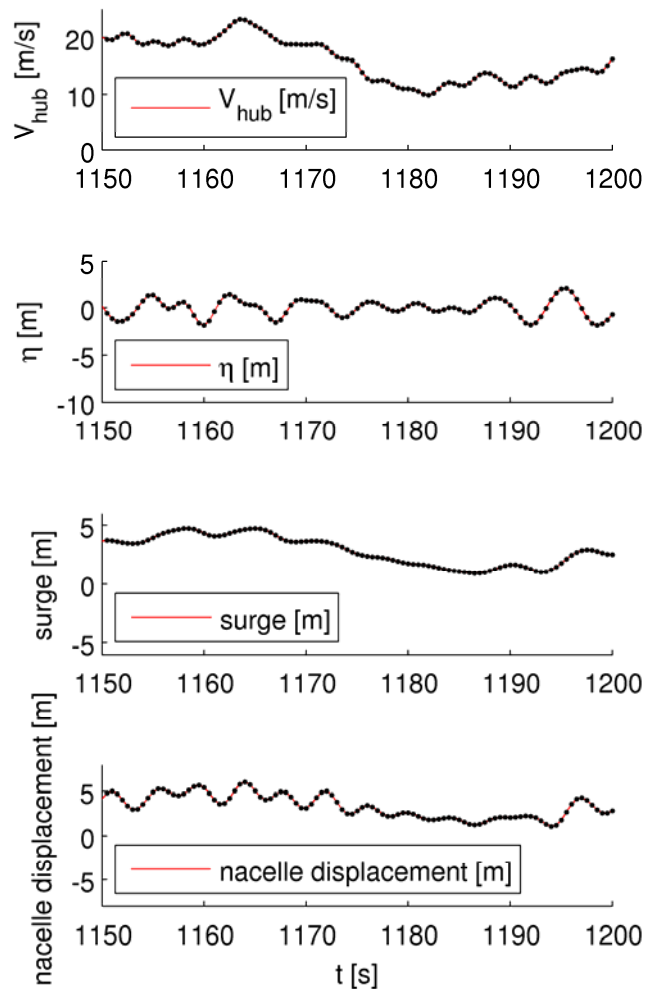


Figure 3.4.4. Comparison of prototype scale results (red line) and model scale results (black dots). The model scale results have been scaled up to prototype scale before plotting.

3.4.7 Consequences of imperfect aerodynamic scaling

To illustrate the consequences of an imperfect reproduction of the aerodynamic loads at model scale, a complementary computation was carried out, with a thrust-curve that deferred from the target curve. The modified thrust curve is shown in Figure 3.4.5 in prototype scale. Further, the response at prototype scale (with correct thrust-curve) and model scale (with imperfect thrust-curve) are compared in the figure. Again, for this comparison, the model-scale results were scaled back to full scale. It is seen how the reduction in the aerodynamic thrust affects the floater and nacelle responses.

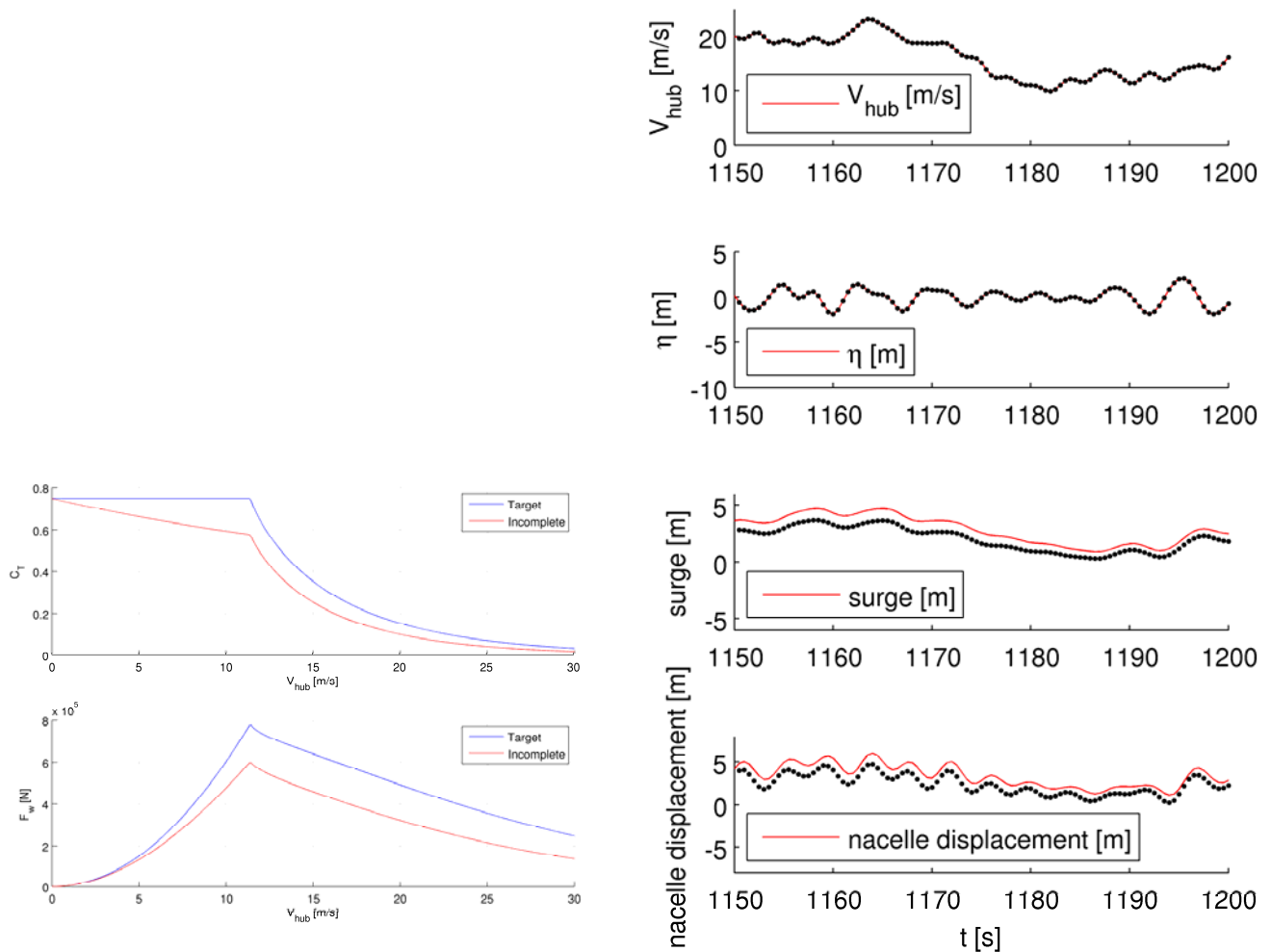


Figure 3.4.5. Consequences of imperfect aerodynamic scaling: Left: Imperfect aerodynamic thrust curve and target thrust curve. Right: Comparison of prototype scale response and model scale response. The model-scale response was produced with the imperfect thrust curve and scaled back to proto-type scale.

3.5 DISCUSSION

Through the example it has been demonstrated that the devised scaling method allows for a perfect reproduction of model response at model scale, provided that the structural loads can be reproduced correctly. This implies a re-design of the blades to the lowered Reynolds number at model scale. The redesigned blades must be able to reproduce the thrust curve of the full scale blades. While the above example only covers the plane motion of the wind turbine, a real wind turbine will also have response in the out-of-plane direction. These can be induced by transverse waves, gyroscopic effects, the dynamic change of rotor moment and through interaction with the mooring system. A true reproduction of these features requires a correct reproduction of the rotor torque as well. This may be difficult to achieve simultaneously with the fulfilment of correct tip speed ratio and thrust curve. In such cases, where a perfect reproduction of the full-scale behaviour at lab scale is not possible, the physical model is of course still valid and 'true' in its own right. It can thus be used to validate a numerical response model, which can later be applied at full scale.

4 CONCLUSIONS AND RECOMMENDATIONS

The present report constitutes the Protocol Manual for ensuring harmonisation of offshore wind and wave simulation being implemented at MaRINET facilities. Wind and wave climates for five offshore wind sites in the North Sea and the Baltic Sea have been presented in terms of probability distributions for wind speed along with a series of lumped sea states and turbulence intensity values, parameterised with respect to the wind speed. Further, extreme values for wind speed and significant wave height have been provided.

Further to the wind distributions and lumped characteristics, the Weibull parameters for the wind distribution and explicit formulas for the turbulence intensity and significant wave height are provided. For the correlation of wave peak period and significant wave height, a standard formula from the IEC-61400-3 code have been found to cover the scatter in the data, although one coefficient in this formula must be decided upon by the user. Further, the value of γ , the JONSWAP peak enhancement parameter must be chosen by the user. This can be done either from an explicit formula or by the standard choices of $\gamma=1.0$ or $\gamma=3.3$. Hereby a full description of a unidirectional wind-wave climate can be constructed. If needed, this climate can be supplemented by the user with the combined directional distribution of wind and waves, either based on data or in terms of parametric studies.

The scaling method proposed is the dynamic-elastic scaling, which maintains the ratios between hydrodynamic, aerodynamic, stiffness-induced and gravitational forces. This scaling preserves the Froude number for the water phase and the tip speed ratio for the rotor. The Reynolds numbers for air and water, however, are not conserved. A redesign of the model-scale blades will therefore be needed. Here the scaled thrust-curve must be matched. Further, if possible, the torque from the airfoil should be matched. This requirement, however, is difficult to achieve due to the change in lift/drag ratio at low Reynolds number. It is therefore foreseen, that the aerodynamic torque and thus produced power will not be scaled correctly. As a consequence, roll-forcing induced by the dynamic change in generator moment will not scale correctly. However, the correct scaling of rotor thrust is found to have higher priority and thus justifies the scaling choice.

An example of down-scaling of wind and wave conditions has been supplied. The example also demonstrates how the structure (a floating wind turbine) should be scaled. It is demonstrated that the proposed scaling yields model-scale results for thrust- and wave- induced motion that can be up-scaled to prototype scale with a perfect match.

5 REFERENCES

1. UpWind: Fisher, T., W. deVries and B. Schmidt: UpWind deliverable, Design Basis WP4: Offshore Foundations and Support Structures - UpWind Project. Universität Stuttgart, 2010.
2. IEC 61400-3: Wind turbines- Part 3: Design of offshore wind turbines, 2009
3. DNV-OJ-J101. OFF SHORE STANDARD: Design of offshore wind turbine structures. DNV, 2007.
4. ABS(American Bureau of Shipping), Offshore Wind Turbine Installation, American Bureau of Shipping, 2010
5. ABS(American Bureau of Shipping), Design Standards for offshore wind farms, American Bureau of Shipping, 2011
6. IEC 61400-1, Design requirements, 2008.
7. IEC 61400-1, Design requirements-amendment1, 2010
8. DS/EN 61400-3, Wind turbines-Part 3: Design requirements for offshore wind turbines, 2009.
9. J.Mann, Wind field simulation, Prob. Engng. Mech. Volume 14, no 4, 269-282, 1998
10. E.R. Jørgensen, S.E. Larsen, S. Frandsen, N.J. Tarp-Johansen and Jenny Trumars, Beatrice Environmental data, Risø-I-2354- FP6 Integrated project DOWNVInd- contract 503202.
11. S. E. Larsen, N. E. Tarp-Johansen, S. Frandsen and E. R. Jørgensen, Södra Midsjöbanken Environmental Data- Initial analysis, Risø-I-2505. FP6 Integrated project DOWNVInd- contract 503202
12. Pena, T. Mikkelsen, S.E. Gryning, C.B. Hasager, A.N. Hahmann, M. Badger, I. Karagali and M. Coutney, Offshore vertical wind shear. Final report NORSEWIND work task 3,1, DTU Wind Energy report 0005 (EN), 2012
13. N. Hahmann, Julia Lange, Alfredo Peña and Charlotte B. Hasager: The NORSEWIND numerical wind atlas for the South Baltic, DTU Wind Energy-E-Report-0011(EN).
14. Karagali, A. Pena, M. Badger and C.B. Hasager, Wind characteristics of the North Sea and the Baltic Seas from QuickScatt satellite. Wind Energy. 2012
15. B M Sumer and J Fredsøe "Hydrodynamics around cylindrical structures". World Scientific 2006.
16. Wierings, J." Shapes of annual frequency distributions of wind speed observed on high meteorological masts. Bound-Layer Meteorol,1988,47,85
17. M.K. Ochi. Ocean waves: the stochastic approach. Cambridge Ocean Technology Series, 2005.
18. Y. Goda. Random Seas and Design Of Maritime Structures. Advanced Series On Ocean Engineering, Volume 15 - World Scientific Publishing Company, 2000.
19. O. Ditlevsen. Stochastic model for joint wave and wind loads on offshore structures. Structural Safety, 24:139163, 2002.



20. P.W. Cheng, G.J.W. van Bussel, G.A.M. van Kuik, and J.H. Vugts. Reliability-based design methods to determine the extreme response distribution of offshore wind turbines. *Wind Energy*, 6:122, 2003.
21. K. Johannessen. Joint distribution for wind and waves in the northern north sea. In *Proceedings of the Eleventh International Offshore and Polar Engineering Conference*, 2001.
22. P. Agarwal, L. Manuel. Simulation of offshore wind turbine response for long-term extreme load prediction. *Engineering Structures*, Volume 31, Issue 10, October 2009, Pages 2236-2246
23. Hildebrant and T. Schlurmann: Breaking wave kinematics, local pressure, and forces on a tripod support structure. *Coastal Engineering*, 1-14, 2012.
24. O. J. Andersen and J. Løvseth: The Frøya database and maritime boundary layer wind description. *Science Direct Marine Structures*, 173-192. 2006.
25. O. J. Andersen and J. Løvseth: Stability modifications of the Frøya wind spectrum. *Journ. Wind Engineering Industrial Aerodynamics*, 236-242, 2010.
26. O. J. Andersen and J. Løvseth: Gale force maritime wind. The Frøya data base. Part1: Sites and instrumentation. Review of the data base. *Jour. Wind Engineering Industrial Aerodynamics*, 97-109, 1995
27. Bottasso, Carlo. "Development of a Wind Tunnel Model for Supporting Research on Aero-Servo-Elasticity and Control of Wind Turbines." Diss. Politecnico di Milano, 2011.
28. Wolowicz , Chester, James Bowman, and William Gilbert. United States of America. NASA. Similitude Requirements and Scaling Relationships as Applied to Model Testing (NASA Technical Paper 1435). Hampton, Virginia: Langley Research Center, 1979.
29. Martin, Heather. METHODOLOGY FOR WINDin/WAVE BASIN TESTING OF FLOATING OFFSHORE WIND TURBINES. University of Maine, June 10-15 2012.
30. Singleton, Jeffrey. "IMPORTANT SCALING PARAMETERS FOR TESTING MODEL-SCALE HELICOPTER ROTORS." Diss. U.S. Army Research Laboratories, Vehicle Technology Center NASA Langley Research Center.
31. Newman, John Nicholas. *Marine Hydrodynamics*. 1. Cambridge: MIT Press, 1977.
32. Dagher, Habib. "Floating Offshore Wind". University of Maine, DeepCwind Consortium. 27 Apr. 2011. Advanced Structures & Composites Center. 25 June 2012.
33. Hall, Stephen. "Dynamic Modeling." *Sport Aviation*. July 1987: 288 - 298.
34. Jameson, Peter. *Innovation on Wind Turbine Design*. Sussex: John Wiley and Sons Ltd., 2011. 78.
35. Anderson, John. *Fundamentals of Aerodynamics*. 4th. Singapore: McGraw-Hill, 2007. 41, 499.
36. Jain, Anant, Amy Robertson, Jason Jonkman, Andrew Goupee, Richard Kimball, and Andrew Swift. United States of America. U.S Department of Energy. FAST Code Verification of Scaling Laws for DeepCwind Floating Wind System Tests. Oak Ridge, TN: Office of Scientific and Technical Information, 2012.
37. Jonkman, J.M. "Dynamics Modeling and Loads Analysis of an Offshore Floating Wind Turbine." Diss. National Renewable Energy Laboratory, 2007.



38. Hansen, AM and Laugesen R "Experimental study of the dynamic response of a TLP wind turbine". BSc thesis, DTU Mechanical Engng. Lyngby, Denmark, June 2012.
39. Jonkman, J, Butterfield, S, Musial, W, Scott, G. "Definition of a 5 MW reference wind turbine for offshore system development". NREL, US, 2009.
40. Matha, D. "Model development and loads analysis of an offshore wind turbine on a tension leg platform with a comparison to other floating wind turbine concepts". MSc thesis. Univ. Colorado, US. April 2009.
41. Hansen, MOL "Aerodynamics of wind turbines". Earthscan, London, UK, 2008.
42. Larsen, TJ and Hanson, TD "A method to avoid negative damped low frequency tower vibrations for a floating pitch controlled wind turbine", Proc. Science Torque Wind. 2007.
43. M Kühn, "Dynamics and design optimisation of offshore wind energy conversion systems," PhD Thesis, Delft University of Technology, Delft, The Netherlands. 2001.
44. J.N. Newman, Marine Hydrodynamics, 1977, MIT Press
45. Morison JR, O'Brien MP, Johnson JW and Schaaf SA "The forces exerted by surface waves on piles". J. Petrol. Techn., Petroleum Transactions, AIME **189** pp 149-154. 1950.